FRAC3DVS-OPG ENHANCEMENTS: SUBGRIDDING, HYDROMECHANICAL DEFORMATION AND ANISOTROPIC MOLECULAR DIFFUSION

NWMO TR-2007-05 **December 2007**

V. Guvanasen

HydroGeoLogic, Inc.

nwmo
NUCLEAR WASTE MANAGEMENT ORGANIZATION
SOCIÉTÉ DE GESTION DES DÉCHETS NUCLÉAIRES

Nuclear Waste Management Organization
22 St. Clair Avenue East, 6th Floor
Toronto, Ontario
M4T 2S3
Canada

Tel: 416-934-9814
Web: www.nwmo.ca

FRAC3DVS-OPG ENHANCEMENTS: SUBGRIDDING, HYDROMECHANICAL DEFORMATION AND ANISOTROPIC MOLECULAR DIFFUSION

NWMO TR-2007-05

December 2007

V. Guvanasen
HydroGeoLogic, Inc.

ABSTRACT

Title: **FRAC3DVS-OPG ENHANCEMENTS: SUBGRIDDING, HYDROMECHANICAL DEFORMATION AND ANISOTROPIC MOLECULAR DIFFUSION**
Report No.: **NWMO-TR-2007-05**
Author(s): V. Guvanasen
Company: HydroGeoLogic, Inc.
Date: December 2007

Abstract

As part of the Nuclear Waste Management Organization's (NWMO) Technical Program, work program activities are being undertaken to further the understanding of groundwater flow system evolution and dynamics within crystalline and sedimentary rock settings. Numerical models applied as part of these activities must be able to effectively simulate flow and transport of radionuclides in deformable, fractured, porous media under variable density and non-isothermal conditions. The FRAC3DVS-OPG code has been used extensively within the NWMO's Technical Program. As part of the ongoing effort to further advance the application of FRAC3DVS-OPG as a flow and transport numerical code, a number of recent improvements have been made including:

(i) coding and application of a previously developed sub-gridding technique;
(ii) incorporation of an approach to better account for the effects of hydromechanical coupling; and
(iii) incorporation of anisotropic molecular diffusion coefficient.

Hydromechanical coupling in the current version of FRAC3DVS-OPG is limited to the case of purely vertical strains with no lateral movements because hydromechanical coupling requires transient hydromechanical stresses as input for all elements within a given simulation domain. Approaches and recommendations to circumvent the above limitation are presented and discussed.

TABLE OF CONTENTS

LIST OF TABLES

Page

LIST OF FIGURES

Page

1. INTRODUCTION

As part of the Nuclear Waste Management Organization's (NWMO) Technical Program, work program activities are being undertaken to further the understanding of groundwater flow system evolution and dynamics within crystalline and sedimentary rock settings. In conducting such studies, a principal focus has been on developing field and numerical geoscience tools and methods to assess groundwater flow system dynamics during the Quaternary (2-0 Ma). In this capacity, numerical methods are being pursued and enhanced to:

i. serve as a systematic framework to assemble and test descriptive concept geosphere models derived from integration of multi-disciplinary data sets;
ii. improve the fidelity with which site characterization data may be input and realized within numerical simulations;
iii. develop methodologies to assess and quantify robustness in numerical flow and transport predictions as a consequence of site characterization uncertainty typical of large Shield flow systems; and
iv. to improve the utility of numerical codes to allow transfer of vetted Site Characterization models to Safety Assessment hence improving Safety Case transparency.

In order to satisfy the above objectives, numerical models used as part of the NWMO's activities must be able to simulate flow and transport of radionuclides in deformable fractured porous media under variable density and non-isothermal conditions. One of the codes that is capable of this type of simulation is FRAC3DVS-OPG (Therrien et al. 2003). As part of the ongoing program to further advance the application of FRAC3DVS-OPG as a flow and transport numerical code within the NWMO, a number of modifications have been made to the code.

In this document, improvements to the FRAC3DVS-OPG numerical code in the following three areas are reported:

i. coding and application of a previously developed sub-gridding technique;
ii. developing and implementing an approach to better account for the effects of hydromechanical coupling on flow system dynamics as affected by the passage of a glacial front, and
iii. incorporating anisotropic molecular diffusion coefficient.

Section 2 provides technical background for the above three areas. Verification examples and discussion are presented in Sections 3 and 4, respectively. A summary and recommendations are given in Section 5.

2. TECHNICAL BACKGROUND

2.1 DESCRIPTION

2.1.1 Subgridding

Many numerical models of groundwater flow and transport use finite-difference or finite-element methods to discretize and solve the governing flow and transport equations. These models often require highly refined meshes in areas of interest where gradients vary rapidly in space to obtain adequate spatial resolution and accuracy. Use of a fine mesh over the entire domain can be computationally intensive, and in some cases intractable (Mehl and Hill 2002). Variably

spaced meshes can lead to elements with large aspect ratios and refinement in areas where such detail is not needed. In addition, fine discretization is advantageous within models in situations where previously constructed mesh geometries render redesign of the entire mesh impractical or not feasible. A solution is to use local grid refinement in which the mesh is refined only in the area of interest.

The need for a locally refined mesh generally is due to three practical requirements (Mehl and Hill 2002):

i. To capture accurately steep hydraulic gradients near pumping or injecting wells
ii. To capture accurately sharp fronts in contaminant transport, and
iii. To represent local hydrogeologic features (e.g., fractures, stratigraphy) as accurately as practicable.

There are two general approaches used in local mesh refinement: model-in-model and direct embedment. A model-in-model approach used by Ward et al. (1987) (referred to as a telescopic mesh refinement in their paper) entailed the use of three successively smaller-scale models: regional, local, and site models. In this case, the approach for inter-scale information transfer has involved linear interpolation, which is associated with several disadvantages. Firstly, coupling between two model meshes occurs only in one direction: from the large mesh to the small mesh. Because there is no feedback from the small mesh to the large mesh, non-linear analyses based on iterative solution techniques are not possible, and significant discrepancies can occur in fluxes or state variables (whichever are not used to couple the meshes) at the model interface. The direct embedment approach is more appropriate for finite-element methods than for finite-difference methods. For finite-difference methods, the choice of neighbouring nodes for finite-difference stencils (5 nodes for two dimensions and 7 nodes for three dimensions) becomes less obvious. Some techniques (e.g., von Rosenberg 1982; Edwards 1996) resulted in poor matrix properties, e.g., asymmetric matrices for the flow equation; and conditional diagonal dominance. These poor properties may not help in reducing computational effort and may even result in divergence of numerical solutions. Assumptions to circumvent these problems may not be realistic (Mehl and Hill 2002). To overcome these problems, some researchers (e.g., Szekely 1998; and Mehl and Hill 2002) developed a variety of hybrid approaches (combinations of model-in-model and direct embedment approaches). However, these approaches require iterative coupling of boundary conditions at model interfaces in an explicit manner.

The local mesh refinement or spatial sub-discretization approach developed for FRAC3DVS-OPG is based on the direct embedment approach. This methodology can be utilized to: (i) eliminate the need for nesting multi-scale models; (ii) permit better integration between engineered barrier systems and the far-field; (iii) improve methods to deal with distinct and/or abrupt changes in hydraulic property distributions; and (iv) closely replicate hydrogeologic features with complicated geometries and orientations.

Information relating to the earlier development of a subgridding methodology for FRAC3DVS-OPG is given by Guvanasen (2005)

2.1.2 Hydromechanical Behaviour

The potential migration of radionuclides between the waste repository horizon and the biosphere may be affected by several processes, including: convection, hydrodynamic

dispersion, sorption, and radioactive decay. In fractured rock, the transport processes are complicated by the fact that complex fracture networks are present in the rock. The host rock surrounding a waste repository may be subjected to in-situ, excavation-induced, thermo-mechanical, and possible future, glacial stresses. These stresses can induce changes in the hydraulic properties of the fractured rock, and along fracture zones, which, in turn, could lead to changes in groundwater flow patterns and transport paths.

Biot (1941) formulated governing equations for the hydromechanically-coupled process with a view to studying three-dimensional consolidation in elastic isotropic materials. Neuzil (2003) presented various formulations for thermohydromechanical coupling in isotropic elastic materials. He also presented formulations for the case of purely vertical strains, in which the deformation equation can be decoupled from the flow and transport equations. By extending the isothermal formulation of Biot, Guvanasen and Chan (2000) developed a theoretical framework for thermohydromechanical coupling with density-dependent solute transport. The framework was subsequently used for the development of a three-dimensional, finite-element code called MOTIF for simulating flow and transport in deformable media that may consist of fractured media with imbedded discrete fractures. The associated analytical expressions are provided in Section 2.2.2.

The formulations for flow and transport within FRAC3DVS-OPG are inherently very similar to those in MOTIF as they are both applicable to porous media imbedded by discrete fractures. However, FRAC3DVS-OPG currently does not have the mechanical component to link to the flow and heat transport components. As shown by Neuzil (2003), when the vertical load is areally homogeneous and lateral strains along the boundary are absent, the thermohydromechanical coupling can be described through the rate of change of vertical stresses in the flow equation. In other words, feedback from the mechanical component is not required.

Because of the unavailability of the mechanical component in the FRAC3DVS-OPG code, the code was modified to accommodate the purely vertical strain case (areally homogeneous vertical stress) only. A discussion relating to possible future enhancement of FRAC3DVS-OPG to account for fully coupled thermohydromechanical processes is given in Section 4.

2.1.3 Anisotropic Molecular Diffusion

Molecular diffusion is a process by which matter is transported from one part of a system to another as a result of random molecular motions. At a macroscopic scale, it may be observed that matter migrates from areas with higher solute concentration to areas with lower solute concentration. This is because there are more solute molecules in the areas with higher solute concentration; therefore there is a net transfer of solute from the higher-concentration areas to the lower-concentration areas as a result of random motions. In the transport processes in porous media, molecular diffusion often occurs simultaneously with mechanical dispersion. The inseparable process is often referred to as hydrodynamic dispersion (Bear 1972) and its analytical expression is provided in Section 2.2.3. When groundwater flow velocity is relatively large, molecular diffusion tends to be much smaller than mechanical dispersion. However, at low flow velocity, molecular diffusion becomes significant.

Anisotropic porous media have different diffusion properties in different directions. In compacted or consolidated sedimentary deposits, pore geometry tends to be directionally dependent, thereby resulting in anisotropic molecular diffusion. The archived version of

FRAC3DVS-OPG assumes that molecular diffusion is isotropic. In this report, a formulation for anisotropic molecular diffusion is given. Based on this formulation, FRAC3DVS-OPG was modified to include anisotropic molecular diffusion.

2.2 FORMULATION

2.2.1 Subgridding

The methodology described below takes full advantage of the existing features in FRAC3DVS-OPG and does not require major changes in the code. A schematic depicting implementation of the subgridding methodology is shown in Figure 2.1.

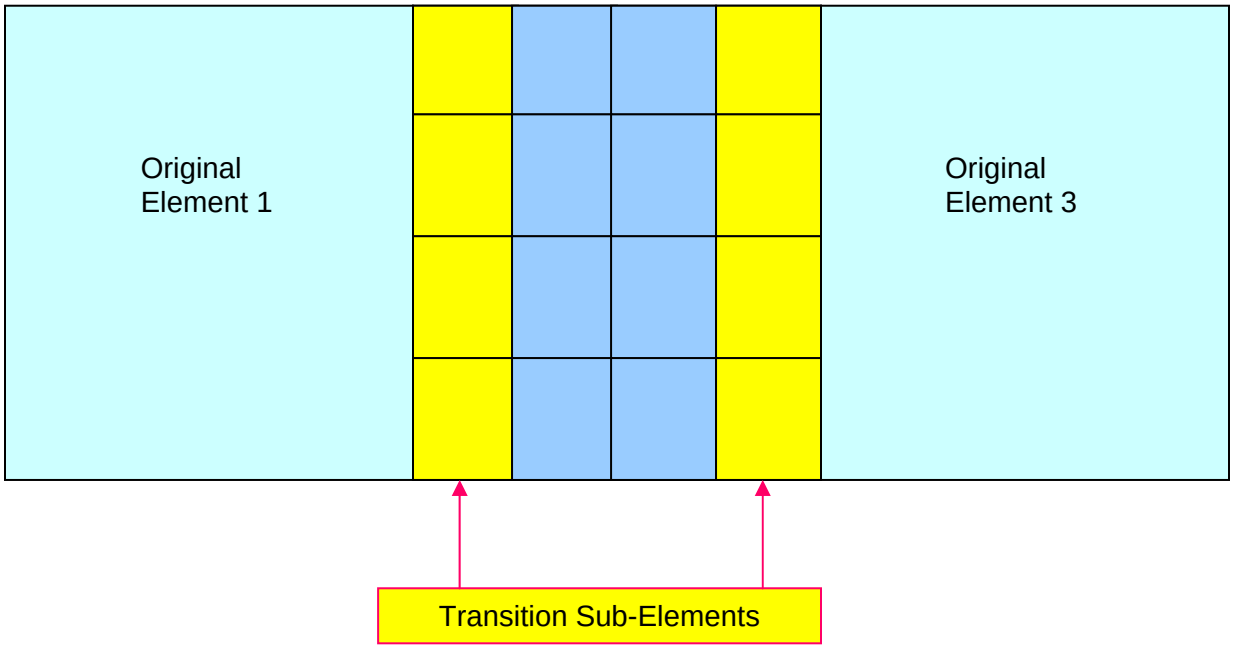

Figure 2.1: Example of Sub-discretization of a 4-noded Plate Element

As shown in Figure 2.1, a 4-noded plate element in the middle of three existing 4-noded parent plate elements is subdivided into 16 sub-elements. The following notation for sub-discretization level associated with an element is used throughout this report: {nx, ny, nz} where nx denotes the number of subdivisions in the x direction, ny denotes the number of subdivisions in the y direction, and nz denotes the number of subdivisions in the z direction. For plate elements, nz is not used. Based on this notation, with x horizontal and y vertical, Elements 1 and 3 that remain un-sub-discretized may be referred to as {1, 1} elements, whereas Element 2 becomes a {4, 4} element. As shown in the figure, the 16 sub-elements within Element 2 may be divided into two categories: interior sub-elements, and transition sub-elements. An interior sub-element has the same properties as the parent element, except for its dimensions. Elemental matrices and vectors of an interior element are generated using the existing subroutines within FRAC3DVS-OPG. A transition sub-element is an element that resides at the interface or contact between a larger (not necessarily an original or parent) element and a smaller element. It shares at least a face with at least one larger neighbouring element or sub-element.

The methodology is relatively general. For instance, Element 2 can be re-discretized into a {6, 6} element or a {10, 10} element. In the past, a unique set of subroutines in the code was required to handle each combination of sub-discretization. The methodology developed for FRAC3DVS-OGP requires only one unique set of subroutines to handle infinite combinations of sub-discretization in two or three dimensions.

An example of sub-discretization in three dimensions is shown in Figure 2.2. As shown in the figure, three existing 8-noded parent block elements may be successively refined in the y and z directions, from left to right.

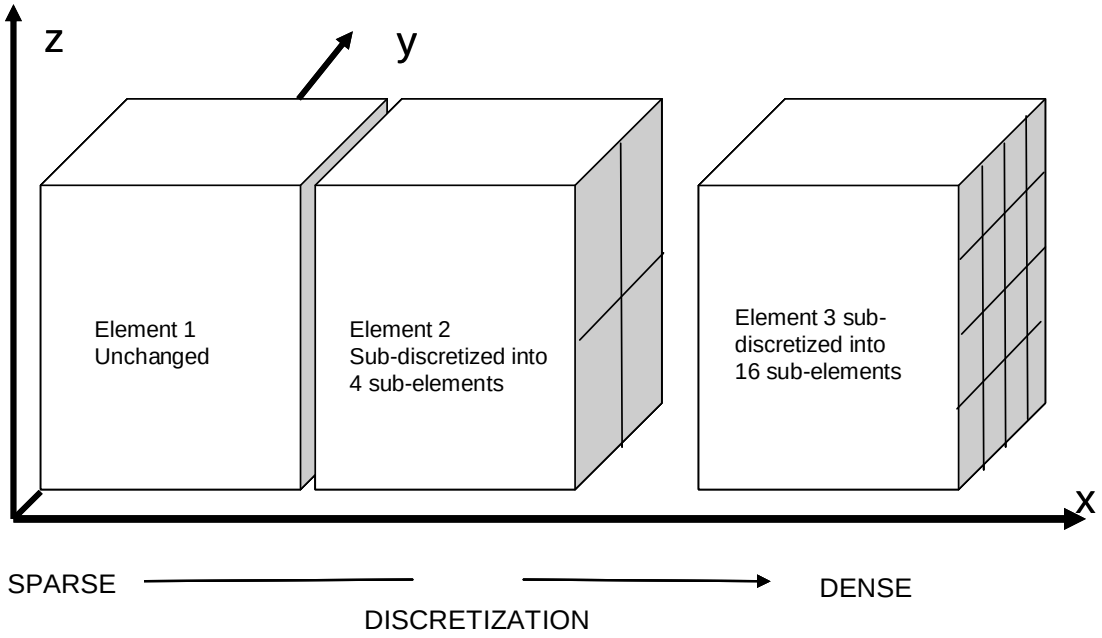

Figure 2.2: Example of Successive Refinement from a Sparsely Discretrized Zone to a Densely Discretized Zone

Element 1 that remains un-sub-discretized may be referred to as a {1, 1, 1} block, whereas Elements 2 and 3 are {1, 2, 2}, and {1, 4, 4} blocks, respectively. In this case, all the sub-elements in Parent Elements 2, and 3 are transition sub-elements because they share at least a face with larger neighbouring elements or sub-elements.

A closer look at an interface between an 8-noded block transition sub-element and a larger element is shown in Figure 2.3. The corner nodes of the shared face of the larger element define the plane. A more specific example is shown in Figure 2.4, where an interface is formed by Nodes 2, 3, 7, and 6. A transition sub-element is defined by Nodes 2, 14, 15, 9, 10, 17, 16, and 11. Nodes 2, 9, 11, and 10 are coplanar with the interface and are referred to as interface nodes.

Along the interface, two conditions must be satisfied: continuity of mass flux across the interface, and continuity of nodal variables at the interface. These two conditions are given below:

Continuity of nodal variables:

$$f_i = T_{iJ} F_J \tag{2.1}$$

Continuity of flux:

$$Q_I = T^*_{Ij} q_j \tag{2.2}$$

where:

f_i = variable *f* at Node *i* of the transition sub-element
F_J = variable *F* at Node *J* of the larger element
q_j = flux *q* at Node *j* of the interface sub-element
Q_I = flux *Q* at Node *I* of the larger element

T_{iJ} and T^*_{Ij} are transformation matrices defined below:

$$T_{iJ} = N_J^{Parent}(\underline{x}_i^{Ise})$$
$$T^*_{Ij} = T_{jI} \tag{2.3}$$

N_J^{Parent} = basis function of Node *J* on the interface of the parent element
x_i^{Ise} = coordinates of interface Node *i* of the transition sub-element

In the example shown in Figure 2.4, variables at nodes 9, 11, and 10 are transformed to variables at nodes 2, 3, 7, and 6.

Treatments of sub-discretization for the flow and transport equations are described in Guvanasen (2005).

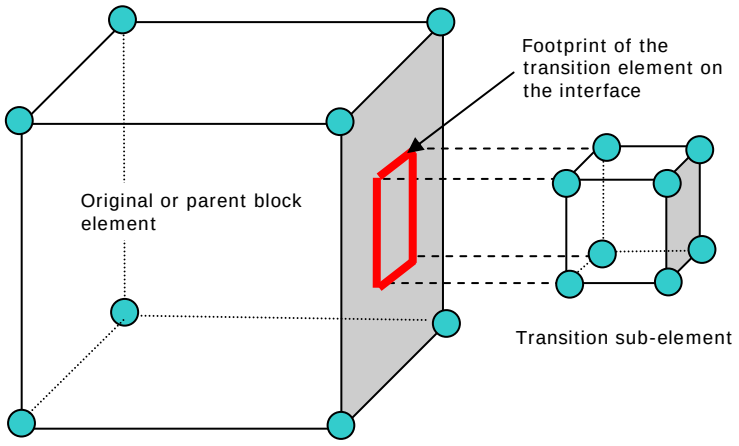

Figure 2.3: Interface Between a Transition Sub-Element and an Adjacent Parent Element

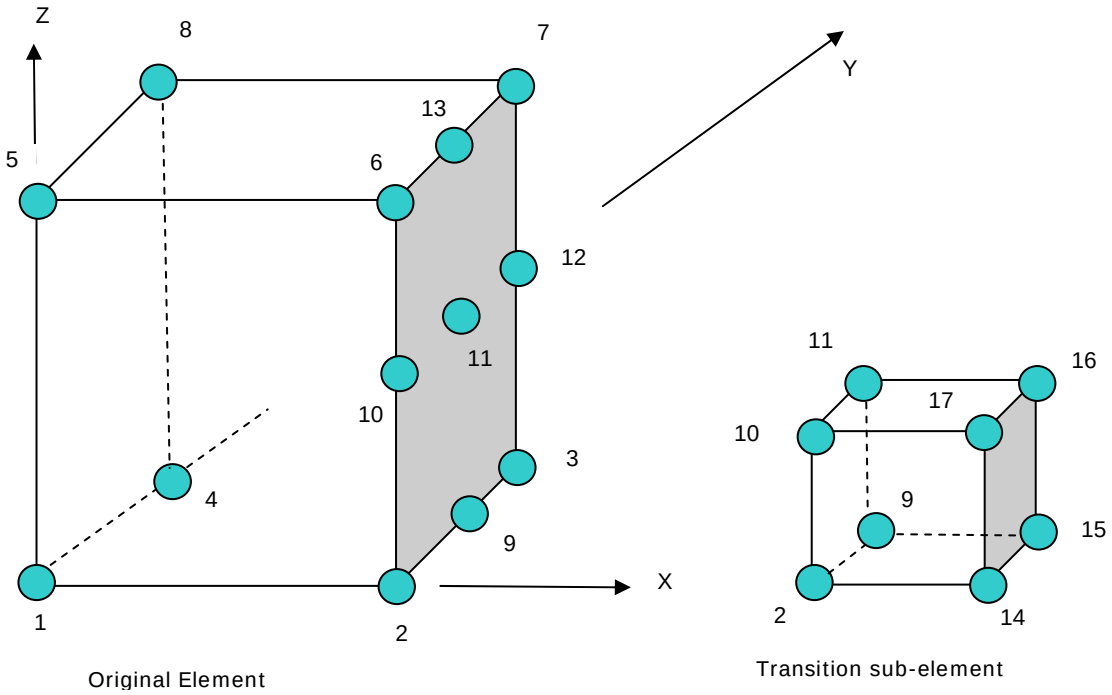

Figure 2.4: Example: An Original or Parent Element Shares a Common Interface with Four Adjacent Transition Sub-Elements (only one transition sub-element is shown)

2.2.2 Hydromechanical Deformation

Generalized equations describing isothermal, hydroelastic equilibrium in poroelastic materials were given by Biot (1941). These equations were subsequently extended to describe thermohydroelastic phenomena by assuming that: 1) the fluid and solid are in thermodynamic equilibrium, and 2) a change in fluid density has no effect on the solid strain. Based on these assumptions, the following equations can be written tensorially (Guvanasen and Chan 2000):

$$e_{ij} = C^{-1}_{ijkl}\left(\tau_{kl} - \tau^{o}_{kl}\right) - \Delta p U_{ij} - \Delta T W_{ij} \tag{2.4}$$

$$e_{ij} = \tfrac{1}{2}\left(\frac{\partial u_i}{\partial x_j} + \frac{\partial u_j}{\partial x_i}\right) \tag{2.5}$$

$$\tau_{kl} = C_{ijkl} e_{kl} + \Delta p U^{*}_{ij} + \Delta T W^{*}_{ij} + \tau^{o}_{ij} \tag{2.6}$$

$$U^{*}_{ij} = C_{ijkl} U_{ij};\; W^{*}_{ij} = C_{ijkl} W_{ij} \tag{2.7}$$

where

e_{ij} = strain tensor,
u_i = deformation in the *i*-th direction,
C_{ijkl} = elastic constant tensor,
τ_{ij} = stress tensor,
τ_{ij}^{o} = initial stress tensor,
U_{ij} = isothermal hydroelastic constant tensor,
W_{ij} = isothermal thermoelastic constant tensor,
x_i = *i*-th direction coordinate,
p = fluid pressure,
p_{ref} = reference fluid pressure,
Δp = $p - p_{ref}$,
T = temperature,
T_{ref} = reference temperature,
ΔT = $T - T_{ref}$.

Note that Equations (2.4) to (2.7) are written based on the assumption that compressive stresses and strains are positive.

The stress expression in Equation (2.6) is used in the following quasi-static equilibrium equation in which the acceleration term is assumed negligible:

$$\frac{\partial \tau_{ij}}{\partial x_j} + F_i = 0 \tag{2.8}$$

where:

F_i = body force in the *i*-th direction (positive upward).

All other variables are defined earlier.

Based on the principle of mass conservation and Darcy's law (Bear 1972), a modified form of Biot's (1955) equation for flow through deformable porous media is written tensorially as (Guvanasen and Chan 2000):

$$\frac{\partial \rho_f \zeta}{\partial t} - \frac{\partial}{\partial x_i}\frac{\rho_f k_{ij} \rho_o g}{\mu_f}\frac{\partial}{\partial x_j}(h + \delta x_3) - \rho_f Q = 0 \tag{2.9}$$

$$\delta = \frac{\rho_f - \rho_o}{\rho_o};\ h = \frac{p}{\rho_o g} + x_3 \tag{2.10}$$

where:

k_{ij}	=	permeability tensor,
t	=	time,
ζ	=	change in volumetric fluid content per unit volume,
ρ_f	=	fluid density,
ρ_o	=	reference fluid density,
g	=	gravitational acceleration,
μ_f	=	fluid dynamic viscosity,
h	=	reference hydraulic head,
Q	=	specific volumetric fluid generation rate, and
x_3	=	coordinate in the vertical direction (positive upward),

All other variables are defined earlier.

For isotropic media, Neuzil (2003) presented Equation (2.6) as:

$$\tau_{ij} = 2Ge_{ij} + \left(2G\frac{\nu}{1-2\nu}e_{kk} + \alpha\Delta p + 2G\frac{1+\nu}{1-2\nu}\alpha_T\Delta T\right)\delta_{ij} + \tau_{ij}^{o} \tag{2.11}$$

and the change in fluid mass ($\rho_f\zeta$) as:

$$\begin{aligned}\rho_f\zeta = &-\rho_o\left(\frac{1}{K}-\frac{1}{K_s}\right)\frac{\tau_{kk}}{3}\\ &+\rho_o\left[\frac{1}{K}-\frac{1}{K_s}+\left(\frac{\theta}{K_f}-\frac{\theta}{K_s}\right)\right]\Delta p-\rho_o\theta_o\left(\alpha_{Tf}-\alpha_{Tp}\right)\Delta T\end{aligned} \tag{2.12}$$

where:

G	=	shear modulus
α	=	hydroelastic constant
α_T	=	linear thermal expansivity
δ_{ij}	=	Kronecker's delta
K	=	bulk modulus of the porous medium
K_s	=	bulk modulus of the solid grains
K_f	=	bulk modulus of fluid
α_{Tf}	=	bulk thermal expansivity of the formation of pores
α_{Tp}	=	bulk thermal expansivity of fluid
θ_o	=	initial porosity
θ	=	porosity
ν	=	Poisson's ratio

All other variables are defined earlier.

Substituting Equation (2.12) into Equation (2.9), one obtains:

$$\frac{\partial}{\partial x_i}\frac{\rho_f k_{ij} g}{\mu_f}\left(\frac{\partial p}{\partial x_j}+\rho_f g\frac{\partial x_3}{\partial x_j}\right)=S_{s3}\frac{\partial p}{\partial t}-S_{s3}\beta\frac{\partial \sigma_t}{\partial t}-\rho_f g\theta\Lambda\frac{\partial T}{\partial t}-\rho_f gQ=0 \tag{2.13}$$

where:

S_{s3}	=	three-dimensional specific storage
β	=	three-dimensional loading efficiency
Λ	=	thermal response coefficient for the fluid-porous medium system
σ_t	=	average total stress

All other variables are defined earlier.

The shear modulus, the hydroelastic constant (α), the three-dimensional specific storage, the three-dimensional loading efficiency, the thermal response coefficient, and the average total stress are defined as:

$$G=\frac{E}{2[1+\nu]} \tag{2.14}$$

$$\alpha=1-\frac{K}{K_s} \tag{2.15}$$

$$S_{s3}=\rho_f g\left[\frac{1}{K}-\frac{1}{K_s}+\left(\frac{\theta}{K_f}-\frac{\theta}{K_s}\right)\right] \tag{2.16}$$

$$\beta=\frac{\frac{1}{K}-\frac{1}{K_s}}{\left[\frac{1}{K}-\frac{1}{K_s}+\left(\frac{\theta}{K_f}-\frac{\theta}{K_s}\right)\right]} \tag{2.17}$$

$$\Lambda=\alpha_{Tf}-\alpha_{Tp} \tag{2.18}$$

$$\sigma_t=\frac{\tau_{kk}}{3} \tag{2.19}$$

where:

E	=	Young's modulus

One can readily see that the equilibrium equation (Equation (2.8)) must be solved simultaneously with the flow equation (Equation (2.13)) and the heat transport equation. For isothermal hydromechanical coupling, one still has to solve the coupled equilibrium and flow equations simultaneously.

Inherent uncertainty about geologic environments and their history has forced researchers to resort to a variety of analytical approaches to approximate hydromechnical coupling effects. One of these approaches is based on an assumption of purely vertical strains (Neuzil 2003). This assumption is based on an observation that lateral gradients in fluid pressure and pressure

changes tend to be small compared to vertical gradients. It is thus often assumed that the resulting deformations can be approximated as purely vertical. Compaction and decompaction due to deposition and erosion often involve load changes that are relatively homogeneous areally, especially when viewed on geologic timescales. In the case of time-varying but areally homogeneous load, the flow equation can be decoupled from the equilibrium equation.

In this case, the lateral strains are assumed to be zero, Equation (2.11) combined with Equation (2.19) can be written as:

$$\sigma_t = \frac{1}{3}\tau_{kk} = \frac{1}{3}\left[\frac{1+\nu}{1-\nu}\tau_{zz} + 2\frac{1-2\nu}{1-\nu}\alpha\Delta p + 4G\frac{1+\nu}{1-\nu}\alpha_T\Delta T + \tau_{kk}^{o}\right] \tag{2.20}$$

Note that Equation (2.20), though different from that of Equation (44) in Neuzil (2003), is equivalent to Neuzil's equation (Neuzil 2007).

Substituting Equation (2.20) into Equation (2.13) yields,

$$\frac{\partial}{\partial x_i}\frac{k_{ij}\rho g}{\mu}\left(\frac{\partial p}{\partial x_j} + \rho g\frac{\partial z}{\partial x_j}\right) = S_s\frac{\partial p}{\partial t} - S_s\zeta\frac{\partial \sigma_{zz}}{\partial t} - \rho g n\Lambda'\frac{\partial T}{\partial t} - gJ \tag{2.21}$$

where:

$$S_s = \left[\frac{1}{K} - \frac{1}{K_s} + \left(\frac{n}{K_f} - \frac{n}{K_s}\right)\right](1 - \lambda\beta) \tag{2.22}$$

$$\lambda = \frac{2}{3}\left(\frac{1-2\nu}{1-\nu}\right)\alpha \tag{2.23}$$

$$\beta = \frac{\frac{1}{K} - \frac{1}{K_s}}{\left[\frac{1}{K} - \frac{1}{K_s} + \left(\frac{n}{K_f} - \frac{n}{K_s}\right)\right]} \tag{2.24}$$

$$\zeta = \frac{\beta(1+\nu)}{3(1-\nu)}\frac{1}{(1-\lambda\beta)} \tag{2.25}$$

$$\Lambda' = \alpha_{Tf} + \frac{\lambda}{\theta} - \alpha_{Tp} \tag{2.26}$$

One can see that the flow equation as portrayed in Equation (2.21) no longer requires the solution of the equilibrium equation as long as vertical stresses can be defined.

The current version of FRAC3DVS-OPG does not have an equilibrium module. An isothermal version of Equation (2.21) (with $\partial T/\partial t = 0$) was implemented.

2.2.3 Anisotropic Molecular Diffusion

Based on the principle of mass conservation, the equation for non-conservative solute transport in porous media can be written (Bear 1972):

$$\frac{\partial}{\partial t}\left[\theta + (1-\theta)K_d \rho_s\right]C + \frac{\partial}{\partial x_i} q_i C \tag{2.27}$$

$$-\frac{\partial}{\partial x_i} D_{ij} \frac{\partial C}{\partial x_j} + \lambda\left[\theta + (1-\theta)K_d \rho_s\right]C - Q_C = 0$$

$$D_{ij} = a_{ijkl} \frac{q_k q_l}{\sqrt{q_m q_m}} + \theta T_{ij} D_d \tag{2.28}$$

For isotropic materials

$$T_{ij} = T\,\delta_{ij} \tag{2.29}$$

where:

C	=	solute concentration,
K_d	=	distribution coefficient,
D_{ij}	=	hydrodynamic dispersion tensor,
T_{ij}	=	tortuosity tensor,
T	=	tortuosity
D_d	=	molecular diffusion coefficient in free water,
λ	=	degradation rate constant, and
Q_C	=	specific solute production rate.

All other variables are defined earlier.

Anisotropy in the mechanical component currently has three components: horizontal longitudinal, horizontal transverse, and vertical transverse. In order to incorporate anisotropy into the diffusion component, tortuosity is directionally dependent, viz:

$$\begin{aligned} T_{11} &= T_x \\ T_{22} &= T_y \\ T_{33} &= T_z \\ T_{ij} &= 0,\ i \neq j \end{aligned} \tag{2.30}$$

where:

T_x	=	tortuosity in the x direction,
T_y	=	tortuosity in the y direction,
T_z	=	tortuosity in the z direction,

2.3 CODE MODIFICATIONS

2.3.1 Subgridding

FRAC3DVS-OPG has been modified to include subgridding capability. In order to make the subgridding component more accessible to general users, the pre-processor for FRAC3DVS-OPG was modified to include a grid generator that can generate imbedded subgrids. The generator assumes that the current grid is the parent grid and resolution refinement in a certain area is required. One-level successive refinement is permitted in the current version of the grid generator. However, the user can incorporate externally-generated, multiple-level, successively- refined grid through a grid input file.

2.3.2 Hydromechanical Coupling

The flow module was modified to include hydromechanical coupling. The current version assumes the purely vertical strain scenario as there exists no mechanical module to provide hydromechanical stresses.

2.3.3 Diffusion Anisotropy

The transport module was modified to include anisotropy in molecular diffusion.

3. VERIFICATION EXAMPLES

3.1 SUBGRIDDING

3.1.1 Example 1.1: Regional Steady-State Groundwater Flow with a Fully Penetrating Injection Well

The purpose of this example is to demonstrate the benefit of subgridding. Several verification examples of the subgridding solution have been presented by Guvanasen (2005) using the modified code.

A small injection well (injection rate = 40 m^3/day) is located in the middle of a square aquifer (4 km x 4 km). The aquifer is 400 metres thick. The well is assumed to be fully penetrating. Because of the symmetry about the y axis, only one half of the domain in the y direction was simulated (see Figure 3.1). Constant-head boundary conditions with head equals 0 metre, were assigned to the boundaries at x = 0 and 4 km. All other boundaries are of no-flow type. Parameter values are given in Table 3.1.

The aquifer was initially discretized into 100, 400 m x 200 m x 400 m brick elements as shown in Figure 3.2a. However, in the vicinity of the well (at (x, y) = (2 000 m, 0 m)), the relatively coarse grid may not simulate appropriately the major rise in potentiometric surface that is likely to be within small distances from the well. To alleviate this problem, the domain in the vicinity of the injection well was subdiscretized as shown in Figure 3.2b, using the methodology discussed in Section 2.2.1, thus avoiding the necessity to remesh the whole domain. Subdiscretization was accomplished through the use of the pre-processor. In Figure 3.2b, elements close to the well are as small as 25 m x 12.5 m x 400 m. Note that because the well is assumed to be fully penetrating, subdiscretization is not necessary in the vertical direction.

A comparison between the solutions based on the parent grid (original grid) and the subdiscretized grid may be made by comparing the head contours shown in Figures 3.3a and 3.3b. As shown in the two figures, the solution based on the subdiscretized grid shows a much greater resolution around the injection well. In addition, the subdiscretized solution also shows the maximum value of potentiometric elevation of 0.017 metres, which is 70 percent greater than that given by the parent grid solution (0.010 metres).

This example highlights the benefits of subgridding, which allows the parent grid to be refined only in regions where high resolution is required.

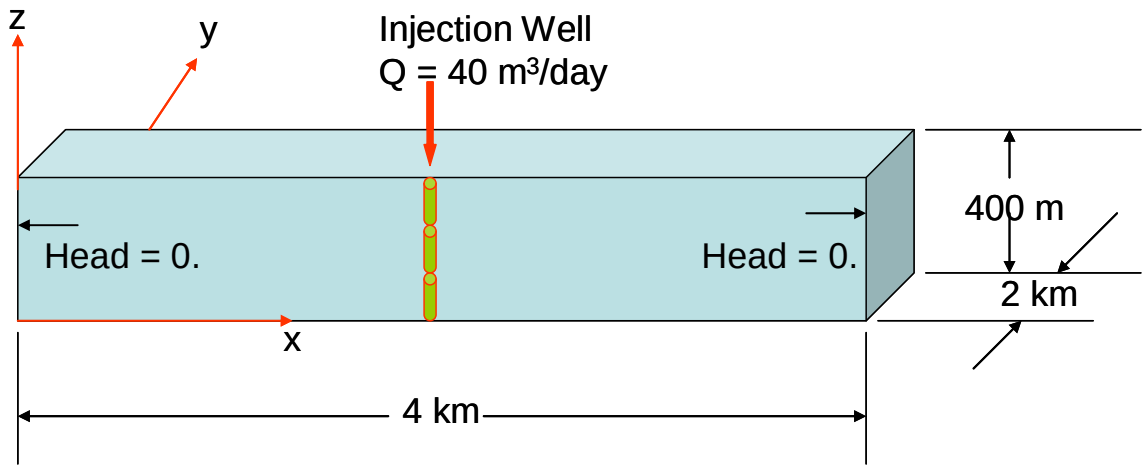

Figure 3.1: Simulation Domain: Example 1.1

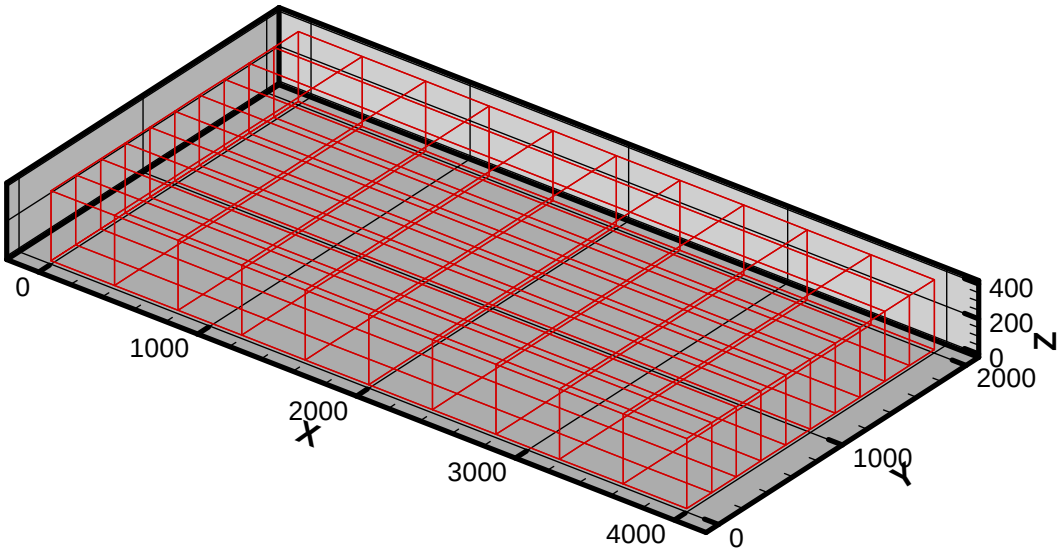

Figure 3.2a: Parent Grid Before Subgridding (in metres)

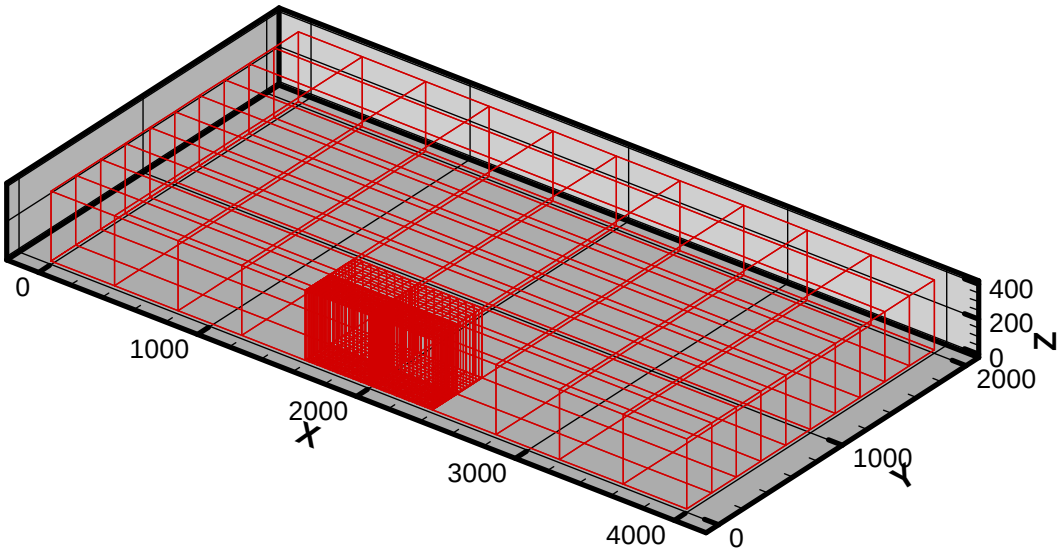

Figure 3.2b: Grid After Subgridding (without vertical subdivision)

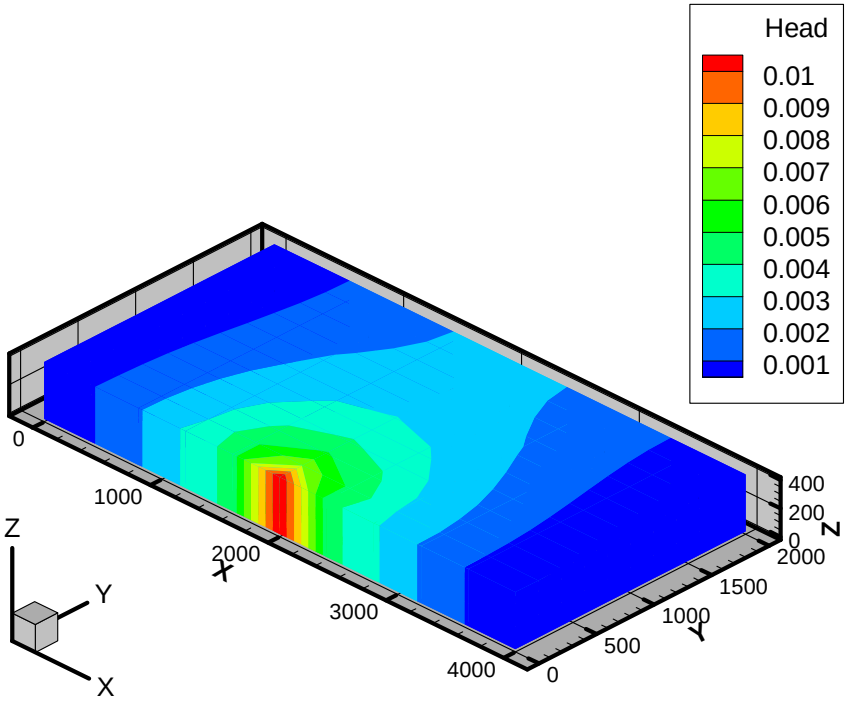

Figure 3.3a: Head (m) Distribution Before Subgridding

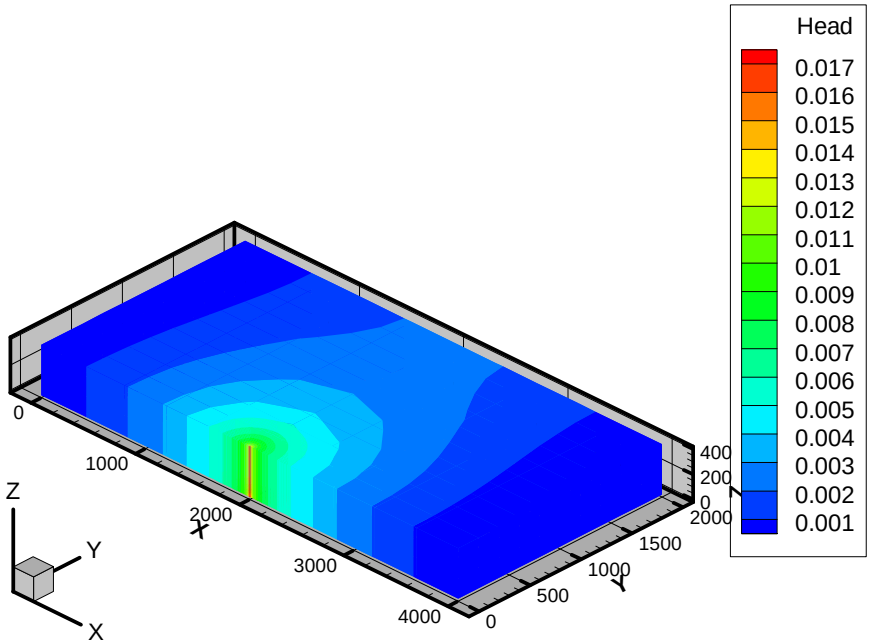

Figure 3.3b: Head (m) Distribution After Subgridding

Table 3.1: Parameter Values: Example 1.1

Parameter	Value	Units
Hydraulic Conductivity	6.42	m/d
Domain length (x direction)	4000	m
Domain width (y direction)	2000	m
Domain thickness (z direction)	400	m

3.1.2 Example 1.2: Regional Steady-State Groundwater Flow with a Partially Penetrating Injection Well

This example is an extension of Example 1.1. In this example, it is assumed the well is relatively shallow and penetrates the aquifer only to the depth of 100 metres from the ground surface. The grid shown in Figure 3.2b was further refined in the vertical direction as shown in Figure 3.4. Elements in the vicinity of the injection well are as small as 25 m x 12.5 m x 100 m. The head distribution for this example that includes the vertically subdiscretized grid is shown in Figure 3.5. As shown, the head distribution is different from that shown in Figure 3.3a and that a distinct three-dimensional distribution of head close to the well is simulated.

This example highlights the benefit of incorporating vertical subdiscretization in regions where high resolution is required, while allowing the parent grid to remain relatively coarse throughout most of the domain, thus minimizing computational effort for the required level of resolution. With the code modifications to incorporate the subdiscretization methodology in Section 2.2.1, the task of subgridding has become more efficient and practical.

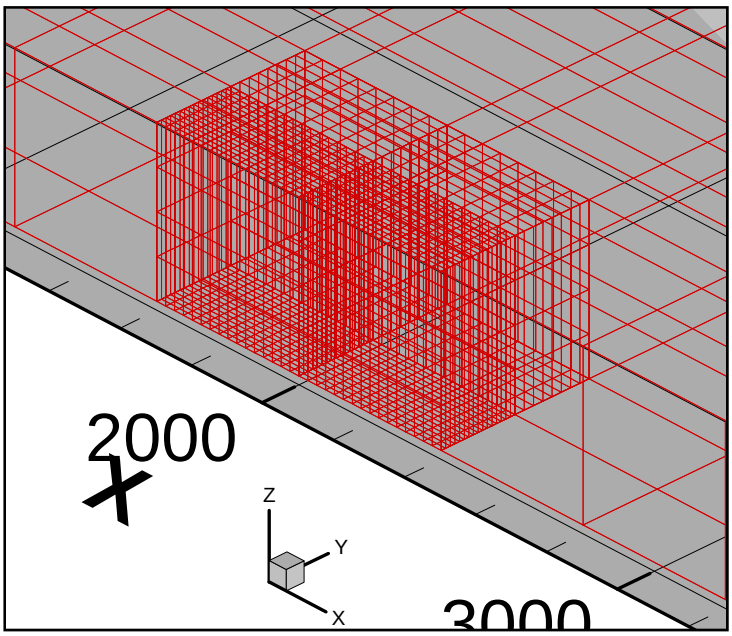

Figure 3.4: Grid after subgridding (with vertical subdivision)

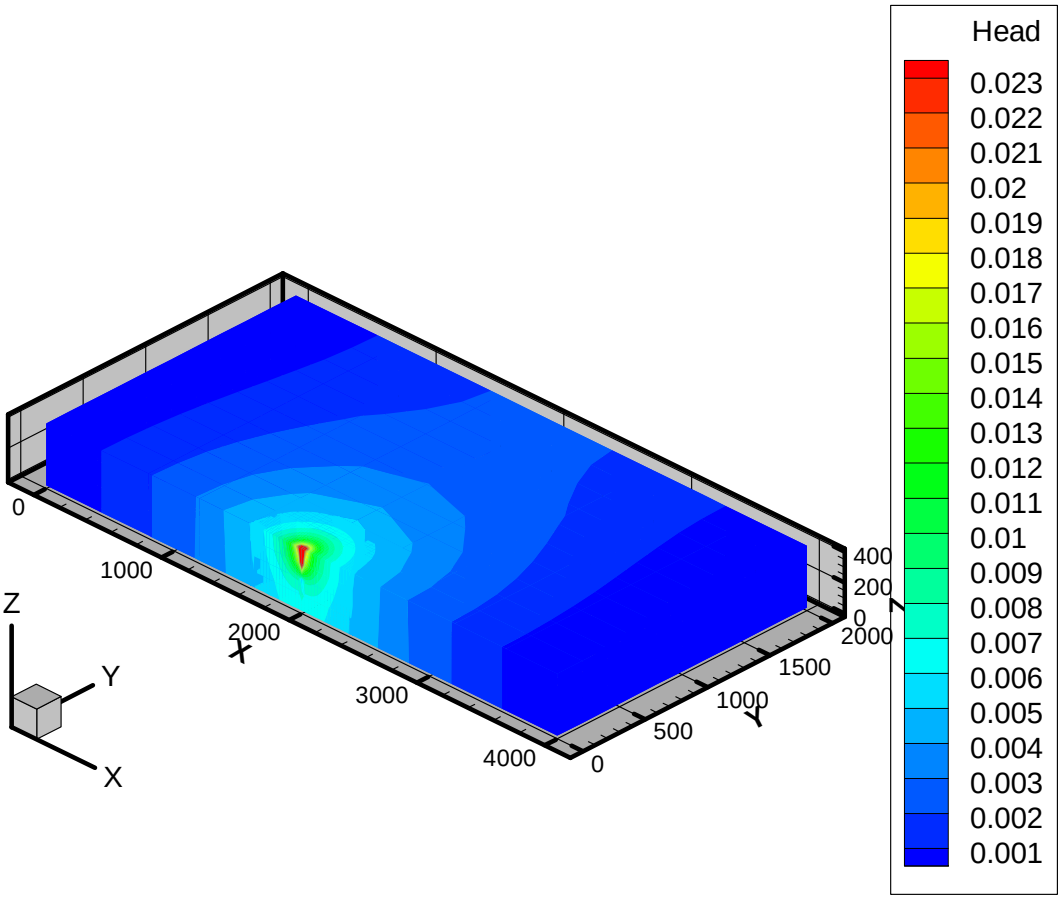

Figure 3.5: Head (m) Distribution After Vertical Subgridding

3.2 HYDROMECHANICAL DEFORMATION

3.2.1 Example 2.1 – A Horizontally Confined Column of Geologic Medium Loaded at Top

This example involves an application of an areally homogeneous vertical load to a column of geologic medium.

As shown in Figure 3.6, a column of geologic medium supporting a load Φ_{zz} and confined laterally in a rigid sheath so that no lateral expansion can occur. It is assumed that no water can escape laterally or through the bottom while it is free to escape at the upper surface.

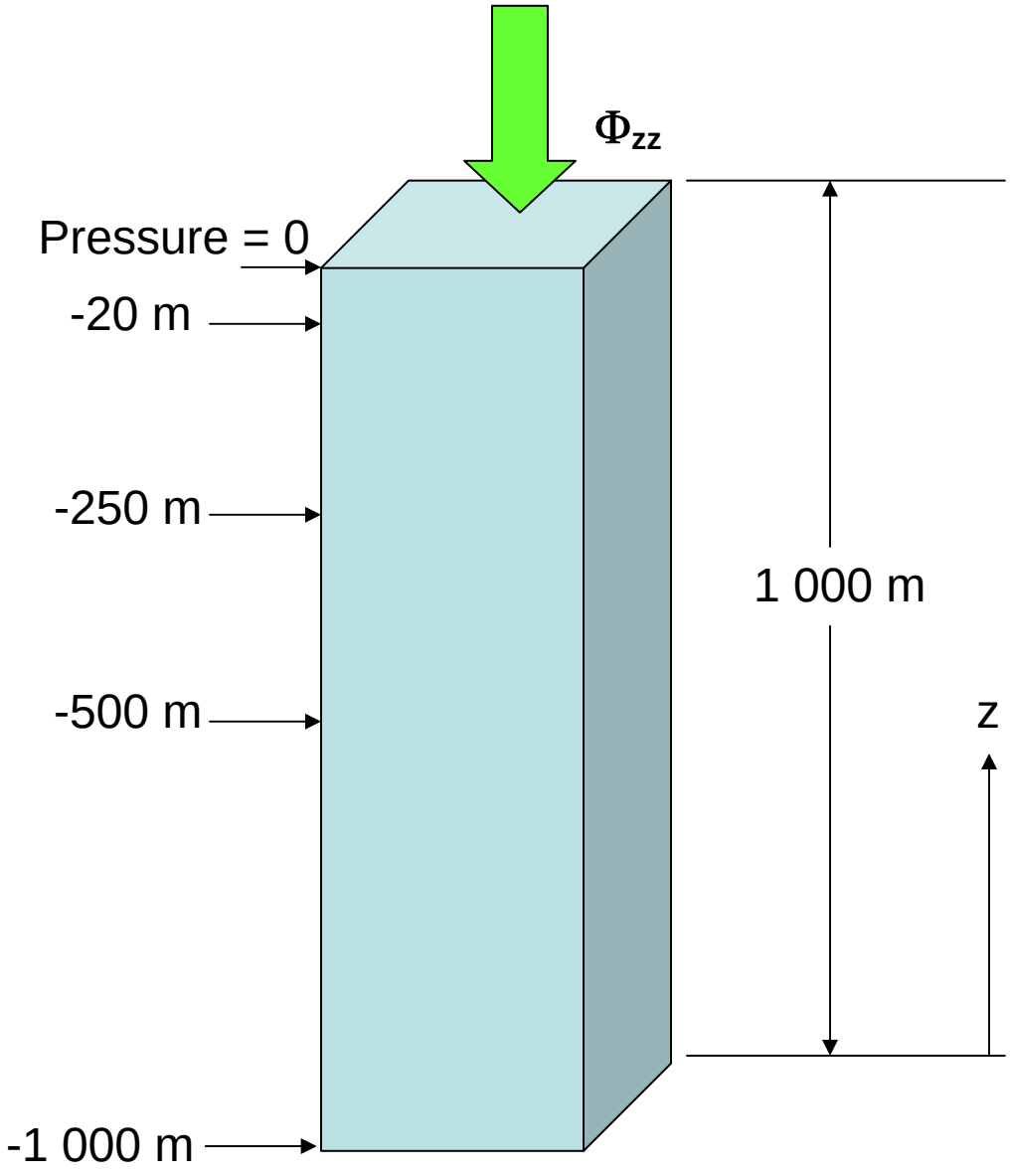

Figure 3.6: A Column of Geologic Medium: Example 2.1

Taking the height of the soil column to be h and z = 0 at the bottom, we have the following boundary conditions:

$$p = 0, \quad for\, z = h$$
$$\frac{\partial p}{\partial z} = 0, for\, z = 0 \tag{3.1}$$

The first condition expresses that the pressure of the water under the load is zero because the permeability of the slab through which the load is applied is assumed to be large. The second condition expresses that no water escapes through the bottom.

The initial condition is that the change of water content is zero when the load is applied because the water must escape with a finite velocity. The initial water pressure at t = 0 based on the foregoing condition is provided by Biot (1941) as shown below.

$$p_0 = \frac{\Phi_{zz}}{K_p\, \rho_f\, g} \tag{3.2}$$

where:

p_0	=	initial pressure head (m)
Φ_{zz}	=	vertical stress (Pa)
K_p	=	Biot's constant (dimensionless – see Biot (1941))
ρ_f	=	fluid density (kg/m^3)
g	=	gravitational acceleration (m/d^2)

Pressure at time t, as given by Biot (1941), is shown below:

$$p = \frac{4 p_0}{\pi} \sum_{n=0}^{\infty} \frac{(-1)^n}{(2n+1)} \exp\left\{ -\frac{K_v}{4 S_S h^2} (2n+1)^2 \pi^2 t \right\} \sin \frac{(2n+1)\pi (z-h)}{2h} \tag{3.3}$$

where:

p	=	pressure head (m)
K_v	=	vertical hydraulic conductivity (m/d)
S_S	=	one-dimensional specific storage (1/d – see Equation (2.21))
h	=	column height (m)
z	=	distance along the z axis (m)

Parameter values are given in Table 3.2. The column height was assumed to be 1 000 metres to reflect the magnitude of depth that FRAC3DVS-OPG is likely to be applied. The vertical stress applied to the surface was assumed to be 0.5 MPa, which causes the water pressure head to rise by 50.9 metres at the onset. The solution above (Equation 3.3) is based on an assumption that the vertical load is instantaneously applied and remains constant thereafter. In applying FRAC3DVS-OPG, it was assumed that the load was increased in a linear fashion from 0 to 0.5 MPa in 1 day. The column was discretized into 100 equal-length elements along the vertical direction. The dimensions of each element in the x and y direction are both 1 metre.

A comparison between the hydromechanically-generated water pressure generated by FRAC3DVS-OPG and Equation (3.3) at several elevations is shown in Figure 3.7 (a-d). As shown in the figures, the agreement between the enhanced FRAC3DVS-OPG code and the analytical solution is very favourable. All the pressure versus time curves indicate that the increase in pressure diminishes to zero at large times.

Table 3.2: Parameter Values: Example 2.1

Parameter	Value	Units
K, Hydraulic conductivity	0.1	m/d
S_s, Specific storage coefficient	0.001	1/m
ζ, Constant in Equation 2.25	1	None
Φ_{zz}, Vertical stress	0.5	MPa
K_p, Biot's constant in Equation 3.2	1	None

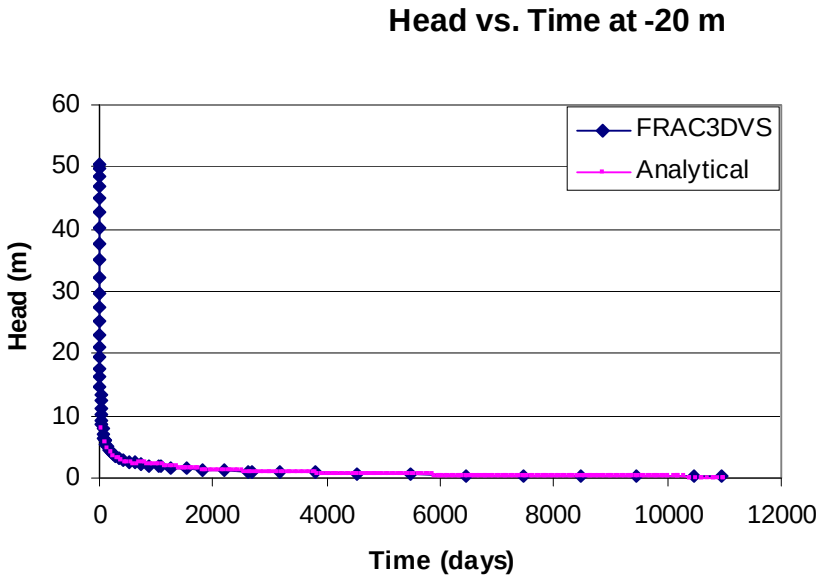

Figure 3.7a: Water Pressure Versus Time at 20 m Below Ground Surface

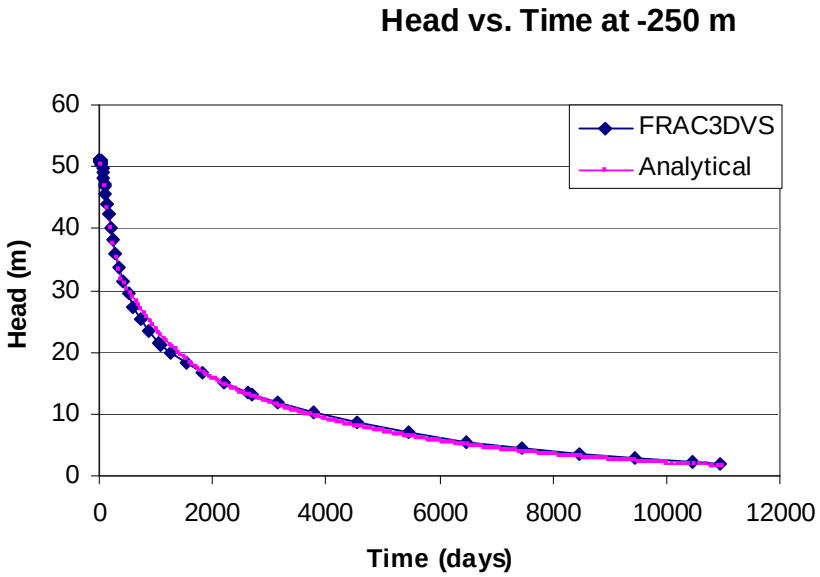

Figure 3.7b: Water Pressure Versus Time at 250 m Below Ground Surface

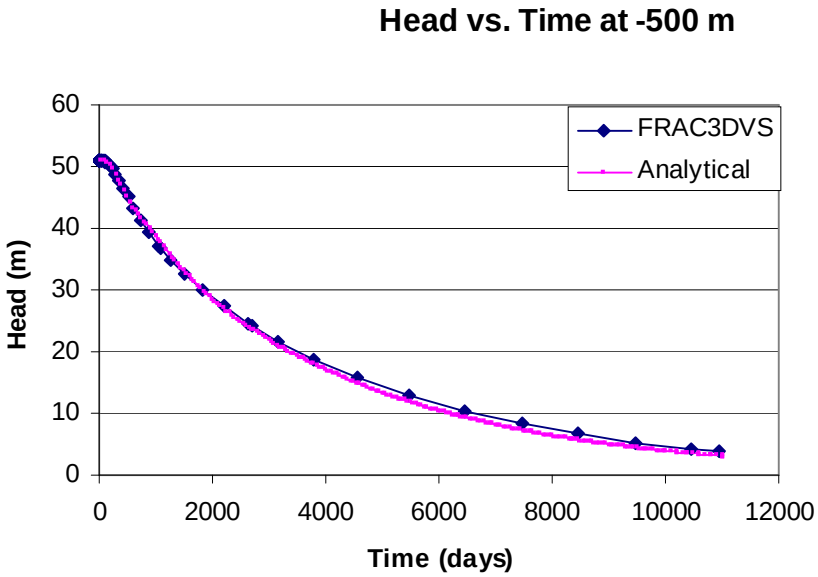

Figure 3.7c: Water Pressure Versus Time at 500 m Below Ground Surface

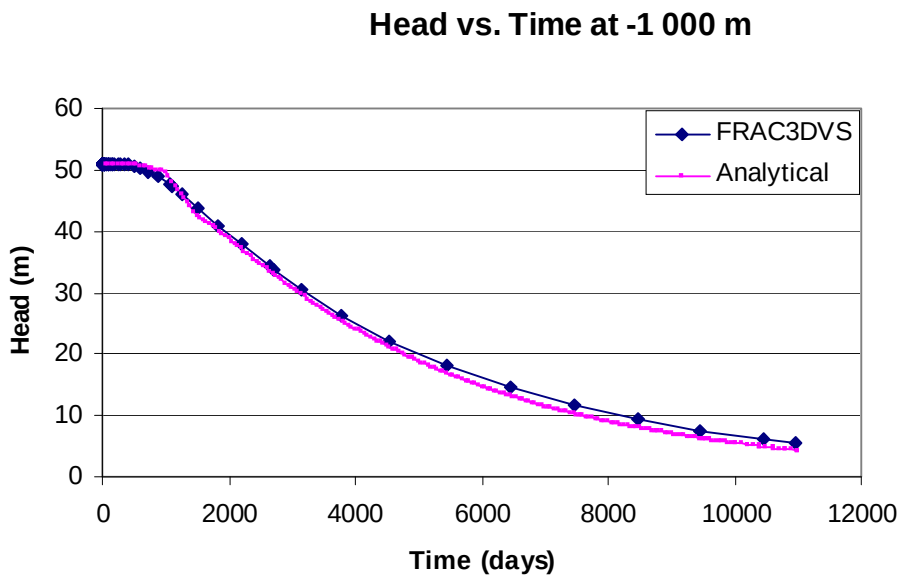

Figure 3.7d: Water Pressure Versus Time at 1 000 m Below Ground Surface

3.2.2 Example 2.2 – Hydromechanical Simulation using FRAC3DVS-OPG with Externally Computed Hydromechanical Stresses

This example is used to demonstrate that FRAC3DVS-OPG could be used in conjunction with other hydromechanical models. Details relating to interaction with other models are given in Section 4. In general, because FRAC3DVS-OPG cannot generate equilibrated hydromechanical total stresses for use in Equation (2.13), the hydromechanical stresses must be generated by other models and used as input for FRAC3DVS-OPG. For this example, material properties are given in Table 3.3.

In the case of Example 2.1, which is a case of purely vertical strains, the average hydromechanical stresses at any time are not required as the flow equation is transformed to implicitly include the hydromechanical effects (Equation 2.21). In order to apply the FRAC3DVS-OPG code to a non-purely-vertical-strain case, time-dependent element-specific total stresses for all elements are required. In this example, total stresses in three dimensions were assumed known. It was further assumed that the settings are identical to those in Example 2.1 so that the total stresses could be computed by Equation (2.20) with water pressure from Equation (3.3). Average hydromechanical stresses versus time at various elevations (from Equations (2.20) and (3.3)) are plotted in Figure 3.8.

Average hydromechanical stresses computed by Equation (2.20) and the flow described by Equation (2.13) were used to generate water pressure at different elevations shown in Figure 3.9 a-d. The agreement between FRAC3DVS-OPG and the analytical solution in Equation (3.3) is an indication that FRAC3DVS-OPG can be interfaced with other hydromechanical models.

Table 3.3: Parameter Values: Example 2.2

Parameter	Value	Units
K, Hydraulic conductivity	0.1	m/d
S_s, Specific storage coefficient	0.0018	1/m
β, 3-dimensional loading efficiency in Equation 2.13	1	None
α, Constant in Equation 2.23	0.4444	None

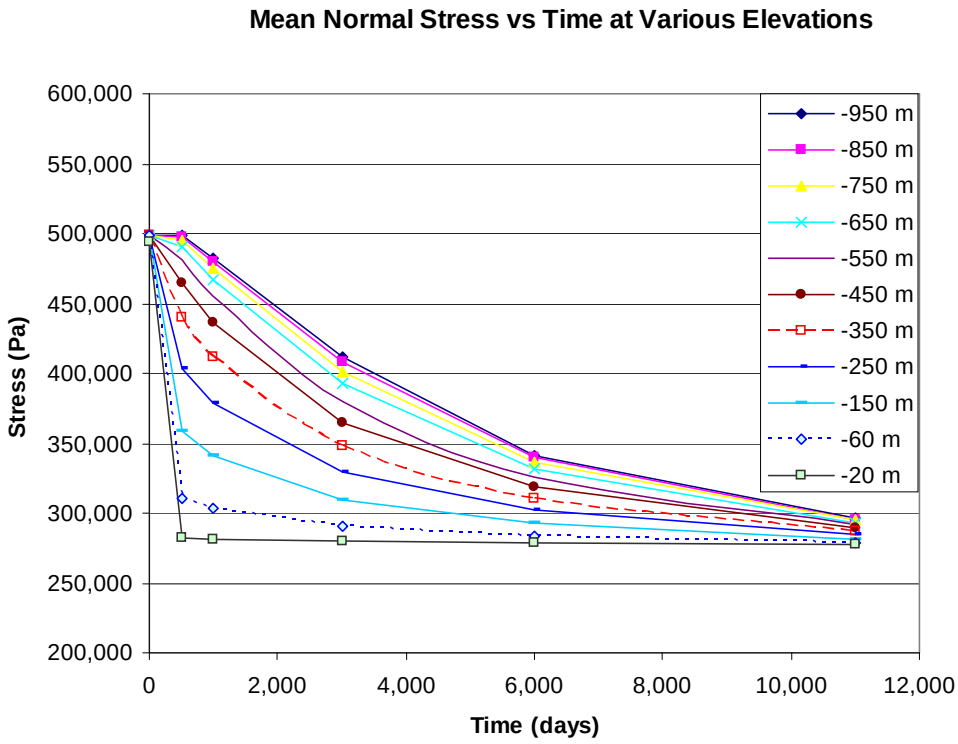

Figure 3.8: Mean Normal Stresses at Different Elevations: Example 2.2

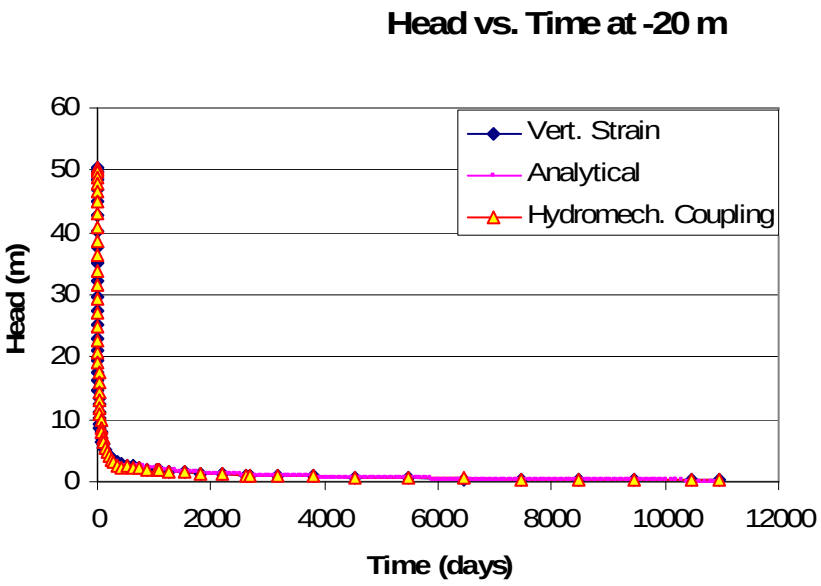

Figure 3.9a: Comparison Between Water Pressures Versus Time at 20 m Below Ground Surface Using Different Methods

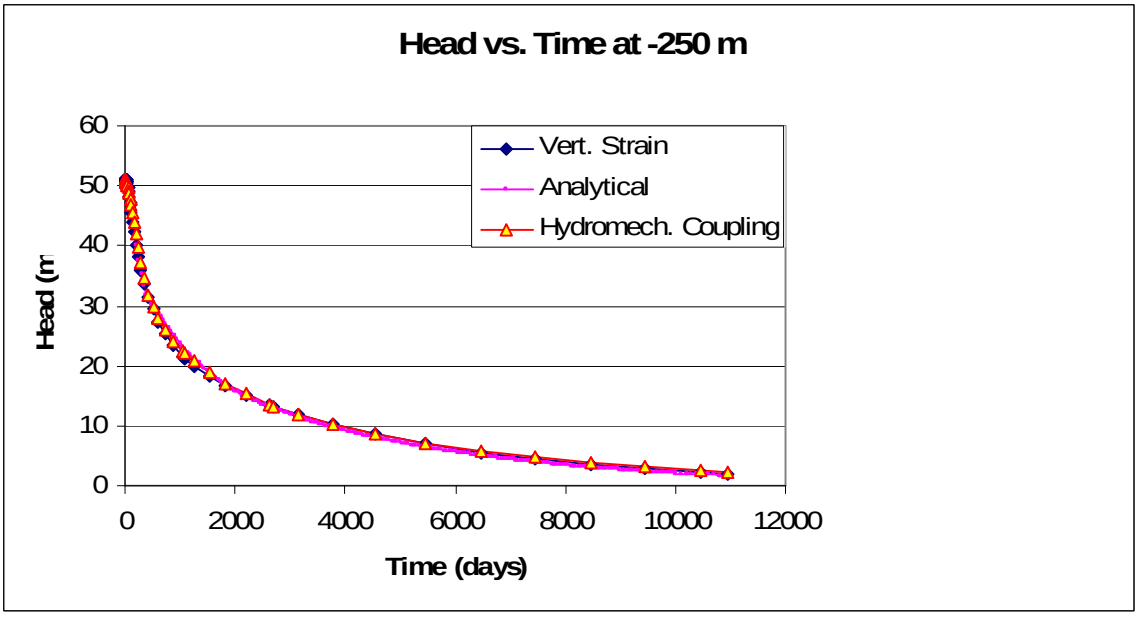

Figure 3.9b: Water Pressure Versus Time at 250 m Below Ground Surface

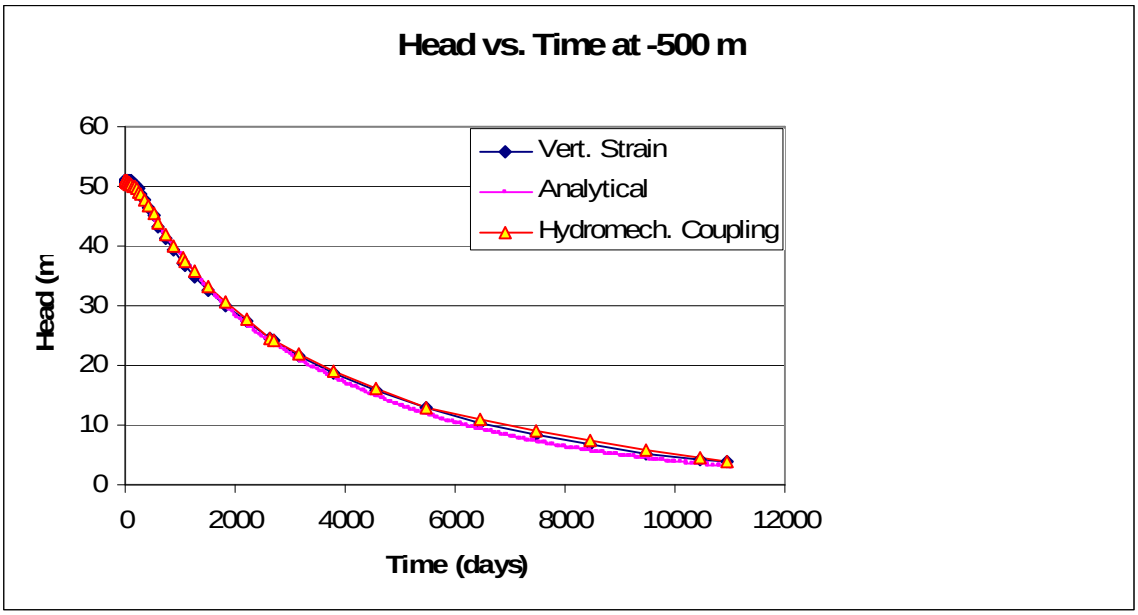

Figure 3.9c: Water Pressure Versus Time at 500 m Below Ground Surface

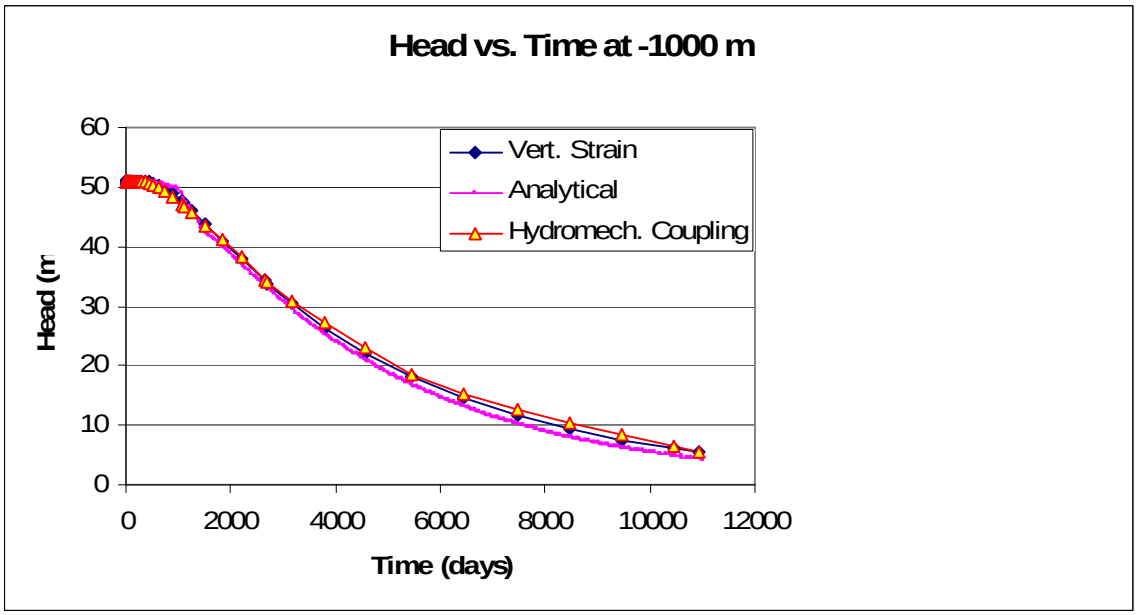

Figure 3.9d: Water Pressure Versus Time at 1 000 m Below Ground Surface

3.3 ANISOTROPIC MOLECULAR DIFFUSION

3.3.1 Example 3.1: Anisotropic Diffusion in Horizontal and Vertical Directions

This example involves anisotropic molecular diffusion in the x and z directions. As shown in Figure 3.10, a domain of 10 metres x 10 metres x 2 metres in dimension was used to verify anisotropic molecular diffusion. Parameter values for this verification case are given in Table 3.4. It should be noted that the vertical diffusion coefficient is 1/100 of the horizontal diffusion coefficient.

Initially, the domain was assumed to be free of solute concentration. For the diffusion in the x direction, a constant concentration was applied to the domain boundary at x = 0. Concentration at time t along the x axis is given by:

$$C = C_o erfc\left(\frac{x}{2\sqrt{D_x t}}\right) \tag{3.4}$$

where:

C_0	=	concentration at the boundary (kg/m^3)
D_x	=	horizontal molecular diffusion coefficient (m^2/d)
x	=	distance along the x direction (m)
t	=	time (d).

A comparison between normalized concentration (C/C_0) versus time curves at 1 metre from the origin of the x axis given by Equation (3.4) and the enhanced FRAC3DVS-OPG code is shown in Figure 3.11a. The agreement between the two solutions is very favourable.

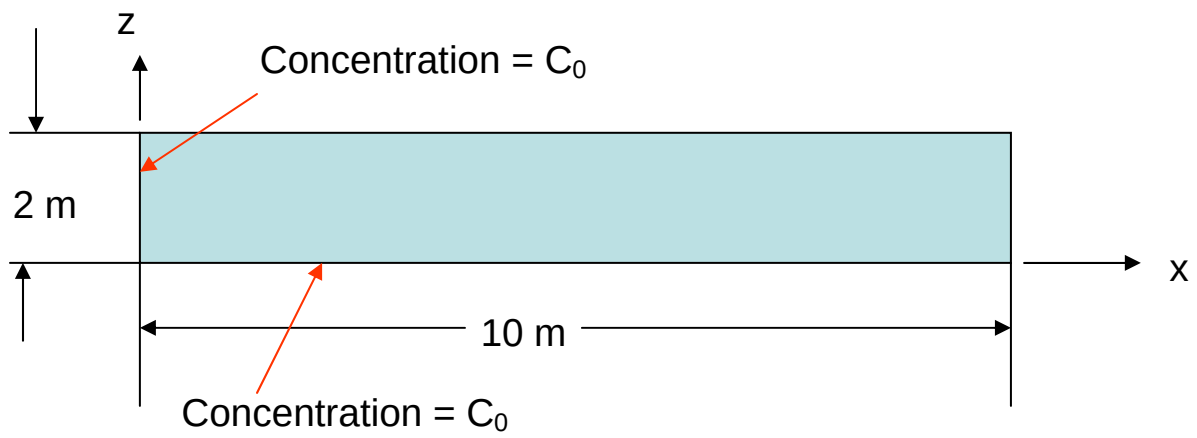

Figure 3.10: Transport Domain. The Thickness in the y Direction is 10 m.

Table 3.3: Parameter Values: Example 2.2

Parameter	Value	Units
Porosity	0.375	None
Free water molecular diffusion coefficient	500	m^2/d
Tortuosity (horizontal component of the tortuosity tensor)	0.1	None
Tortuosity (vertical component of the tortuosity tensor)	0.001	None

Diffusion in the vertical direction was initiated by assigning a constant concentration boundary to the domain boundary at z = 0. Concentration at time t along the z axis is given by:

$$C = C_o erfc\left(\frac{z}{2\sqrt{D_z t}}\right) \tag{3.5}$$

where:

D_z = vertical molecular diffusion coefficient (m^2/d)
z = distance along the z direction (m)

A comparison between normalized concentration versus time curves at 1 metre from the origin of the z axis given by Equation (3.5) and the enhanced FRAC3DVS-OPG code is shown in Figure 3.11b. The agreement between the two solutions is very favourable. Concentration distributions caused by horizontal and vertical diffusion at 1 day are shown in Figures 3.12a and 3.12b, respectively. It is apparent that diffusion in the horizontal direction is much greater than its counterpart in the vertical direction.

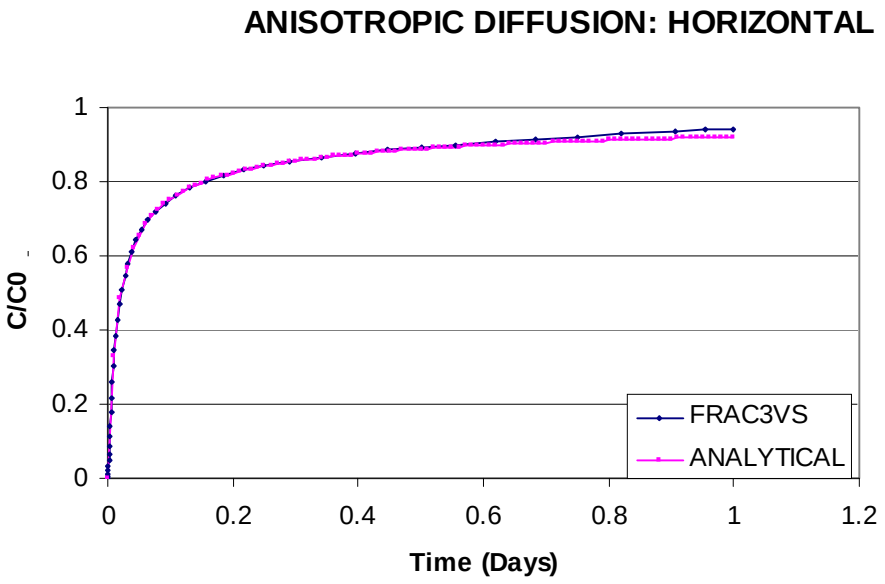

Figure 3.11a: Normalized Concentration vs Time at 1 m from the Constant Concentration Boundary

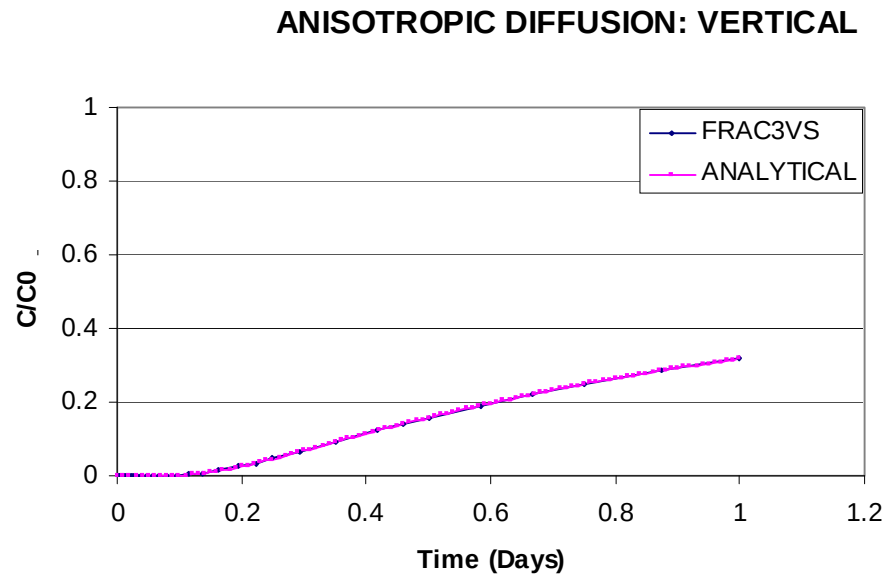

Figure 3.11b: Normalized Concentration vs Time at 1 m Above the Constant Concentration Boundary

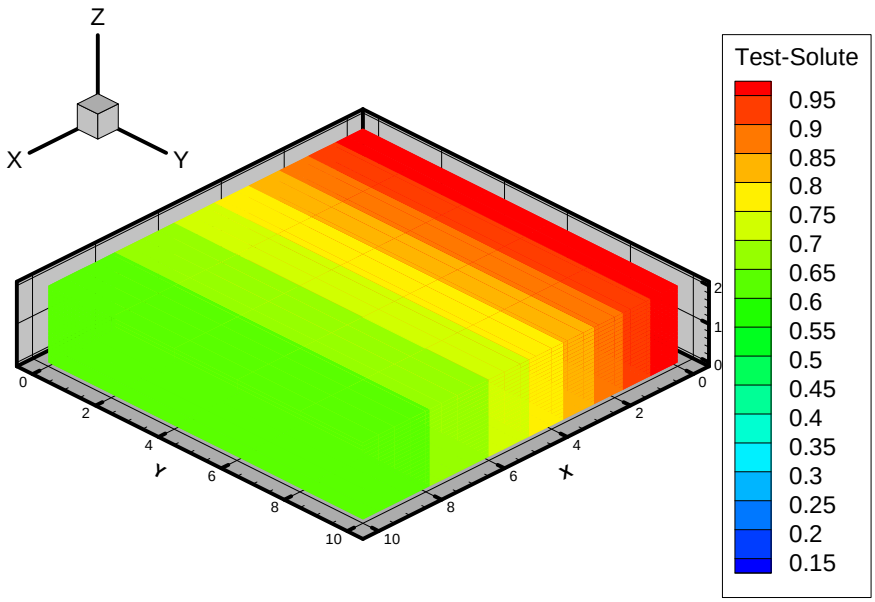

Figure 3.12a: Normalized Concentration Distribution at 1 day with Horizontal Diffusion

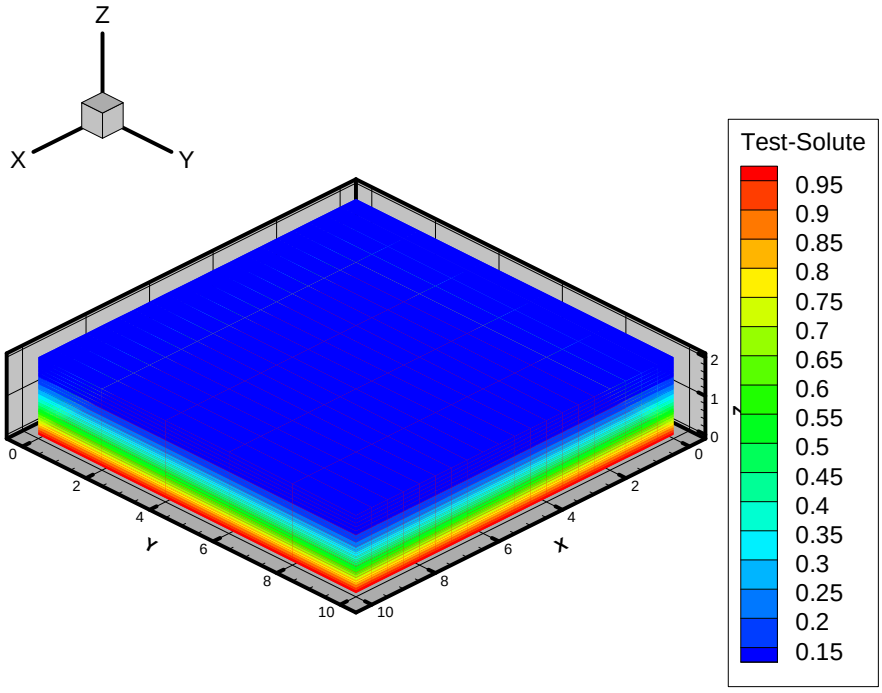

Figure 3.12b: Normalized Concentration Distribution at 1 day with Vertical Diffusion

4. DISCUSSION

4.1 ENHANCEMENT OF THERMOHYDROMECHANICAL CAPABILITY IN FRAC3DVS-OPG

The current hydromechanical coupling implemented in FRAC3DVS-OPG is limited to the scenario of purely vertical strain with lateral constraints. This scenario corresponds to the case of areally homogeneous vertical loading. In practice, the assumption of areally homogeneous vertical loading may be violated in many instances where significant changes in local stresses can occur. Examples of these instances include: in the vicinity of a glacial front; near a glacial terminus where the glacial thickness (therefore vertical loading) varies; and thermal stresses arising from radiogenic heat in the vicinity of spent fuel containers. The case of a glacial front is discussed further below.

Figure 4.1(a) shows an area that is partially covered by a glacial front. A stress distribution in the underlying geologic medium resulting from the assumption of purely vertical strains is also shown as vertical arrows directly below the ice sheet. In the figure, it can be seen that the impact of the advent of a glacial front is not felt beyond the ice sheet. In reality, owing to the Poisson effects, lateral stresses are developed beyond the glacial front, as shown in Figure 4.1(b). The stress distribution beyond the glacial front could be very complex and extended over a large distance from the glacial front (on the order of several kilometres). At shallow depths, tensile stresses could develop as a result of bulging upward of the geologic medium. Shown in Figure 4.1(c) is a comparison between the changes in hydraulic head ascribed to the vertical strain assumption (in Figure 4.1(a)) and to the stress distribution in Figure 4.1(b), which is caused by the Poisson effects. It can be seen that the change in hydraulic head with the Poisson effects precedes that due to the purely vertical strain assumption. Further, the change in hydraulic head underneath the glacier for the case with the Poisson effects is not as severe as that for the case with the purely vertical strain assumption because the leading hydraulic front has time to dissipate prior to the arrival of the glacial front. Poisson effects can also occur behind the tail end of a glacier. In this case, the change in hydraulic head in the vicinity of the glacial end for the case with the Poisson effects is not abrupt because the trailing hydraulic front has time to dissipate after the departure of the glacier. Based on this observation, it is clear that, in order to accurately describe the hydromechanical or thermohydromechanical effects, the FRAC3DVS-OPG code must be enhanced to include a module that could be used to simulate mechanical deformation. In doing so, there are several possible options. The options that are germane to FRAC3DVS-OPG are described below.

The first option is diagrammatically summarised in Figure 4.2. This option requires that a thermohydromechanical (THM) code be run prior to a given FRAC3DVS-OPG simulation. Because there is no feedback between the two codes, it is necessary that the thermohydromechanical code simulate the chosen scenario completely so that information relating to stresses and velocities could be passed on to the FRAC3DVS-OPG code via external files. The velocity information could be utilized in the transport module within FRAC3DVS-OPG. However, one major drawback is that, the potential technical /theoretical differences between FRAC3DVS-OPG and a THM code (e.g., finite-difference versus finite-element methods, parameters and formulation of flow and transport equations) may give rise to mass balance errors within FRAC3DVS-OPG. A possible remedy for this weakness is to use FRAC3DVS-OPG to simulate both flow and transport using the hydromechanically or thermohydromechanically equilibrated stresses from the thermohydromechanical code. However, this remedy requires that the flow and transport simulation be repeated, thereby making the run very time consuming and computationally demanding. This option simply

requires that FRAC3DVS-OPG be minimally modified to accept stresses and velocities from an external thermohydromechanical code (see Figure 4.2).

To address the disadvantages associated with Option 1, Options 2 and 3 were also examined. These options are diagrammatically summarised in Figures 4.3 and 4.4, respectively. Option 2 requires that a thermohydromechanical code be used as part of the iterative solution process within FRAC3DVS-OPG. During each iteration, stress information from the thermohydromechanical code is accessed via external files. In this case, it means that FRAC3DVS-OPG has to terminate the current run and write all the current information on files so that it can be run subsequent to the run of the external thermohydromechanical code in a restart mode with additional information from the thermomechanical portion of the code. This method is computationally inefficient as numerous successive runs are required. Furthermore, each run requires that all simulation information (geometry, boundary conditions, parameters, etc.) be read in anew, and at the end of a run all state variables (deformation, stresses, head, temperature, and concentration be written to restart files. The restart files must be read in by respective codes at the beginning of each run. In order to address this problem, Option 3 (see Figure 4.4) was considered. With this option, a mechanical module (preferably as a dynamic-link library (DLL) module) is required to be embedded in the FRAC3DVS-OPG code. With this configuration, information can be efficiently transferred internally from module to module via memory without interruption. It will be necessary to request a DLL version of the code from the code's vendor.

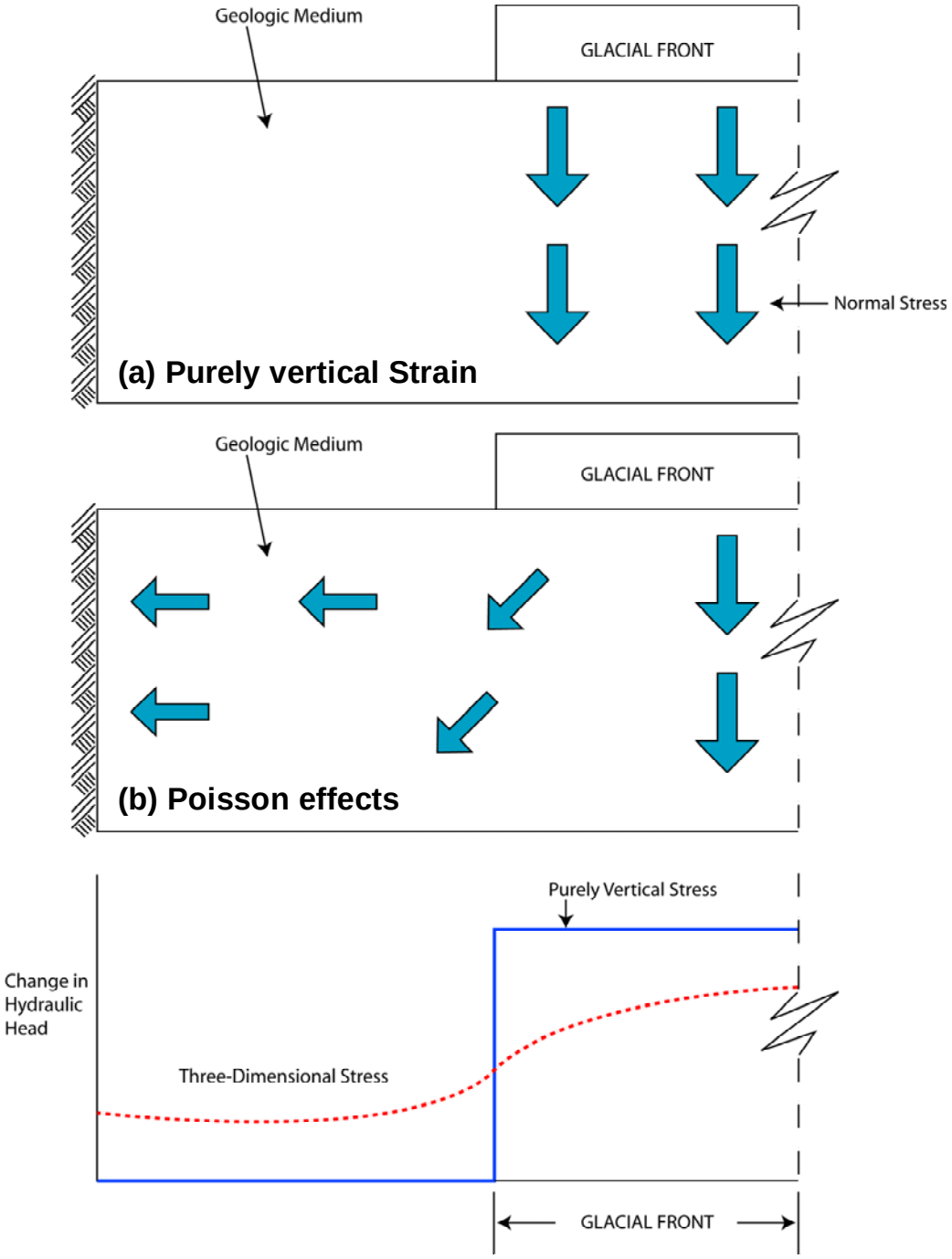

Figure 4.1: Comparison Between Purely Vertical Strain and a General 3D Hydromechanical Coupling Scenario

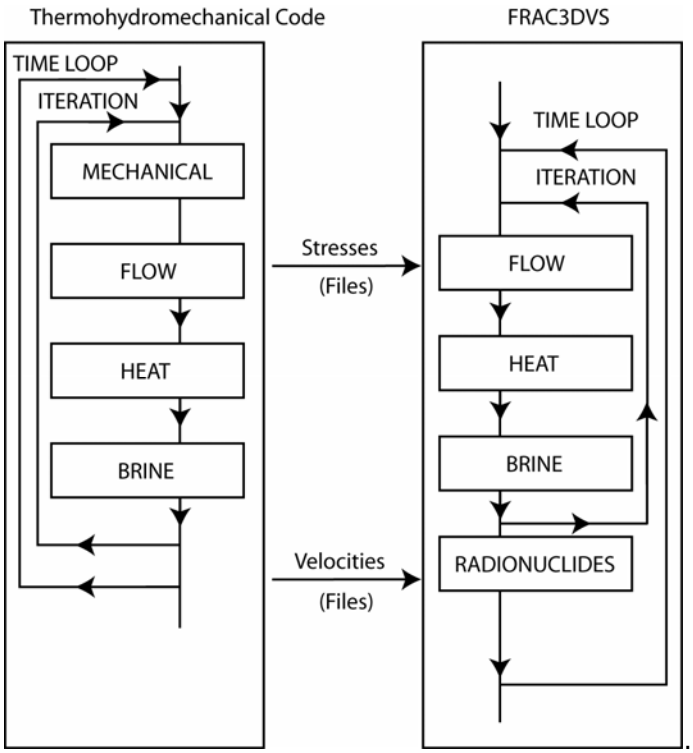

Figure 4.2: Thermohydromechanical Coupling: Option 1

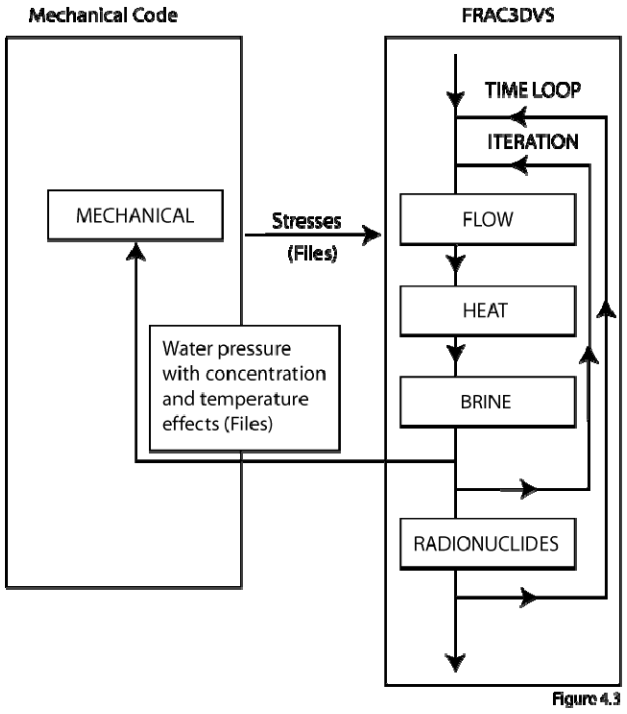

Figure 4.3: Thermohydromechanical Coupling: Option 2

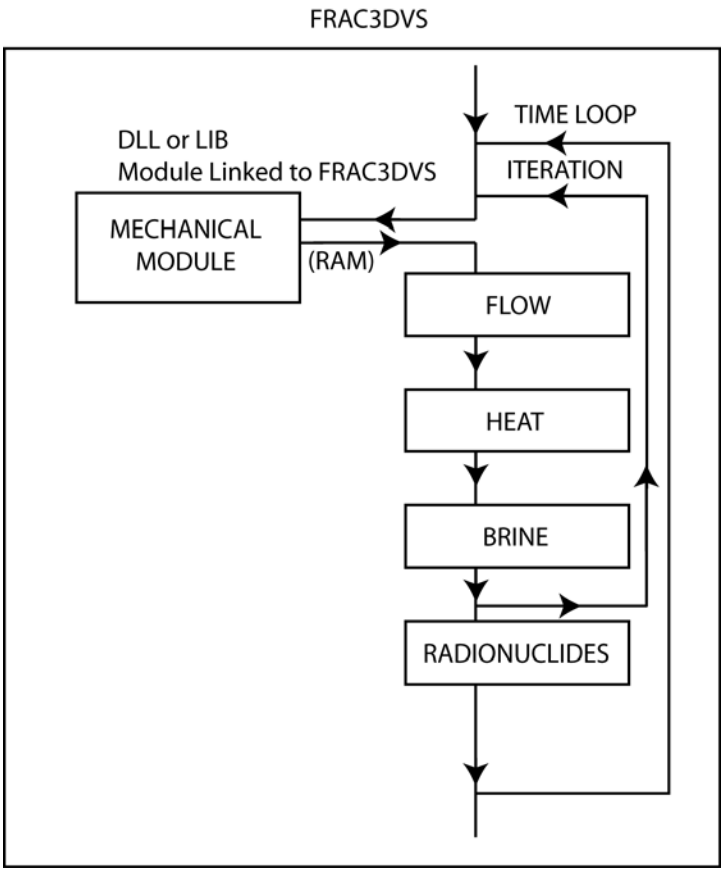

Figure 4.4: Thermohydromechanical Coupling: Option 3

4.2 THERMOHYDROMECHANICAL SOLUTION PROCEDURE

Incorporation of a three-dimensional mechanical module into FRAC3DVS-OPG is a major step as the module requires memory approximately one order of magnitude greater than that for a flow or (one-species) transport module. For this reason, it is essential that a computationally efficient scheme be applied for thermohydromechanical coupling.

The analysis of heat, fluid flow, and solute transport through a fully saturated, deforming (fractured) porous media represents a field problem with four degrees of freedom. The most obvious solution procedure of the four coupled equations is to solve for deformation, hydraulic head, temperature, and concentration simultaneously. This approach is known as the monolithic approach, first proposed by Lewis and Karahanoglu (1981). This approach results in an asymmetric coefficient matrix for the combined equation after discretization in time. Another solution technique consists of partitioning the combined system of equations after the integration in the time domain. This procedure is known as algebraic partitioning. It is well known that a great number of partitions are possible in four-field problems. Matrix partitioning, together with staggered or simultaneous solution schemes, plays an important role in the design of numerical models for coupled problems. The standard staggered procedure has been described and analyzed in the literature (Schlefler 1985). It is essentially an iterative method of the Gauss-Seidel type that can be used to solve large, coupled sets of algebraic equations resulting from a discretization of the appropriate field equations.

The advantage of the staggered procedure is that it permits a sequential solution of the equations, allowing the use of available numerical codes for simpler problems (simplified through partitioning). The main concept of the staggered strategy is to begin by solving a block of equations for the first set of field variables while the other variables remain fixed. The remaining block of equations are then solved for the second set of field variables while the updated first variables are kept fixed. This procedure is performed through an appropriate partitioning of the matrices on the left-hand side and transferring components to the right-hand side of the equation.

Extensive numerical experiments on consolidation problems (Matteazzi *et al.* 1996) have shown that staggered solutions are in general only advantageous if the coupling is weak. In the case of non-isothermal consolidation where the coupling with the temperature field tends to be weak, the displacement and pressure fields are solved implicitly while partitioning is used between these two fields and the temperature field.

The implication of the above approach is that the flow and mechanical components should be solved in a monolithic fashion, whilst the remaining two components (solute and heat transport) can be solved sequentially in a staggered fashion. Currently in FRAC3DVS-OPG, the three components (flow, solute transport, and heat transport) are solved in the standard staggered procedure in conjunction with Picard iteration. For FRAC3DVS-OPG, if at all possible, hydromechanical coupling should be formulated in a monolithic sense, whilst the remaining two components require no changes.

Based on this premise, the hydromechanical enhancement of FRAC3DVS-OPG should be divided into two phases: Phase I – development of a monolithic hydromechanical module outside FRAC3DVS-OPG; and Phase II – incorporation of the hydromechanical module into FRAC3DVS-OPG in a staggered sense. In Phase I, the module must be developed in such a way that it can be used as a Fortran-callable subroutine in FRAC3DVS-OPG. This module should be developed and tested independently outside the FRAC3DVS-OPG environment so that its characteristics (computational requirements, convergence characteristics, etc.) can be ascertained before incorporating it into FRAC3DVS-OPG in Phase II. The module is expected to be embedded in the manner shown in Figure 4.4 with the mechanical and flow modules combined.

5. SUMMARY AND RECOMMENDATIONS

5.1 SUMMARY

Improvements to the FRAC3DVS-OPG numerical code have been made in the following three areas: (i) coding and application of a previously developed sub-gridding technique; (ii) incorporation of simplified hydromechanical coupling, and (iii) incorporation of anisotropic molecular diffusion.

Hydromechanical coupling in the current version of FRAC3DVS-OPG is limited to the case of purely vertical strains with no lateral movements because true hydromechanical coupling requires transient, equilibrated, hydromechanical stresses as input. In the current version of the code, there exists no mechanical module to provide these hydromechanical stresses. A recommendation to enhance the hydromechanical capability of FRAC3DVS-OPG is given below.

5.2 RECOMMENDATIONS

As stated in Section 4.2, for FRAC3DVS-OPG, hydromechanical coupling in the code should be formulated in a monolithic sense to ensure computational stability and efficiency as the coupling between deformation and fluid flow is relatively strong. Changes to the thermal and solute transport components are not required.

It is therefore recommended that the hydromechanical enhancement of FRAC3DVS-OPG be divided into two phases: Phase I – development of a monolithic hydromechanical module outside FRAC3DVS-OPG; and Phase II – incorporation of the hydromechanical module into FRAC3DVS-OPG in a staggered sense. Details of these two phases are given in Section 4.2.

6. REFERENCES

Bear, J. 1972. Dynamics of Fluids in Porous Media. American Elsevier.

Biot, M.A. 1941. General Theory of Three-Dimensional Consolidation. J. Applied Physics, 12(2):155-164.

Biot, M.A. 1955. Theory of Elasticity and Consolidation in a Porous Anisotropic Solid. J. Applied Physics, 26(2):182-185.

Edwards, M.G. 1996. Elimination of adaptive grid interface errors in the discrete cell-centered pressure equation. Journal of Computational Physics. Vol. 126: 356-372.

Guvanasen, V. and T. Chan, 2000. A three-dimensional numerical model for thermohydromechanical deformation with hysteresis in a fractured rock mass. International Journal of Rock Mechanics and Mineral Sciences, 37, 89-106.

Guvanasen, V. 2005. FRAC3DVS enhancements: development and implementation of spatial sub-discretization methodology. Report No: 06819-REP-01300-10113-R00. Ontario Power Generation, Nuclear Waste Management Division, Toronto, Ontario, Canada, M5G 1X6. July 2005

Huyakorn, P.S., S.D. Thomas and B.M. Thompson. 1986. Techniques for making finite-elements competitive in modeling flow in variability saturated porous media. Water Resources Research. Vol. 20(8): 1099-1115.

Lewis, R.W., and N. Karahanoglu, 1981. Simulation of Subsidence in Geothermal Reservoirs. In Numerical Methods in Thermal Problems, Vol. II, R.W. Lewis, K. Morgan, and B.A. Schlefler (eds.), Pineridge Press, Swansea, Wales, pp. 326-335.

Lewis, R.W., and B.A. Schrefler, 1998. The Finite-Element Method in the Static and Dynamic Deformation and Consolidation of Porous Media. John Wiley and Sons.

Matteazzi, R., B.A. Schlefler and R. Vitaliani, 1996. Comparison of Partitioned Solution Procedures for Transient Coupled Problems in Sequential and Parallel Processing. In Advances in Finite Element Technology, B.H.V. Topping (ed.) , Civil-Comp Press, Edinburgh, pp: 351357.

Mehl, S., and M.C. Hill. 2002. Development and evaluation of a local grid refinement method for block-centered finite-difference groundwater models using shared nodes. Advances in Water Resources. Vol. 25: 497-511.

Neuzil, C.E., 2003. Hydromechanical Coupling in Geologic Processes. Hydrogeology Journal, 11:41-83.

Neuzil, C.E., 2007. Personal communication.

Panday, S.M., P.S. Huyakorn, R. Therrien and R.L. Nichols. 1993. Improved three-dimensional finite-element techniques for field simulation of variability flow and transport. Journal of Contaminant Hydrology. Vol. 12: 3-33.

Schrefler, B.A., 1985. A Partitioned Solution Procedure for Geothermal Reservoir Analysis. CANM (Communications in Applied Numerical Methods), Vol. 1, pp. 53-56.

Sykes, J.F., S.D. Normani and E.A. Sudicky. 2003a. Regional scale groundwater flow in a Canadian Shield setting. Ontario Power Generation. Nuclear Waste Management Division Report No. 06819-REP-01200-10114 R0. Toronto, Canada.

Sykes, J.F, S.D. Normani, E.A. Sudicky and M.R. Jensen. 2003b. Modelling strategy to assess long-term regional-scale groundwater flow within a Canadian Shield setting. Proceedings 4th Joint IAH/CGS Conference, September 29-October 1, 2003. Winnipeg, Canada.

Szekely, F. 1998. Windowed spatial zooming in finite-difference groundwater flow models. Ground Water. Vol. 36(5): 718-721.

Therrien, R., E.A. Sudicky and R.G. McLaren. 2003. FRAC3DVS: An efficient simulator for three-dimensional, saturated-unsaturated flow and density-dependent, chain-decay solute transport in porous, discretely fractured porous or dual porosity formations. University of Waterloo. Waterloo, Canada.

von Rosenberg, D.U. 1982. Local mesh refinement for finite difference methods. Paper SPE 10974 presented at the 57th Society of Petroleum Engineers Annual Fall Technical Conference, September 26-29, 1982. New Orleans, U.S.A.

Voss, C.I. 1985. SUTRA – A finite-element situation model for saturated-unsaturated fluid-density-dependent groundwater flow with energy transport or single species solute transport. U.S. Geological Survey Water Resource Investigation Report No. 84-4369. Reston, U.S.A.

Ward, D.S., D.R. Buss, J.W. Mercer and S.S. Hughes. 1987. Evaluation of a groundwater corrective action at the Chem-Dyne Hazardous Waste Site using a telescopic mesh refinement modeling approach. Water Resources Research. Vol. 23(4): 603-617.